Modeling of multi-component flows with phase transition and application to collapsing bubbles*

Ee Han, Maren Hantke and Siegfried Müller

Preprint No. 409   **October 2014**

Key words: multi-component fluids, non-equilibrium model,
               phase transition, relaxation process, bubble collapse

AMS Subject Classifications: 76Txx, 74Sxx, 76T10

Institut für Geometrie und Praktische Mathematik

RWTH Aachen

Templergraben 55, D-52056 Aachen, (Germany)

Modeling of multi-component flows with phase transition and application to collapsing bubbles *

Ee Han, Maren Hantke, Siegfried Müller

October 10, 2014

Abstract

The classical two-phase flow model of Baer and Nunziato is generalized to a thermodynamic consistent multi-component model in multi dimensions. The extended model allows to deal with phase transitions where exchange processes are modeled by relaxation terms. In particular, chemical relaxation is based on chemical potentials instead of Gibbs free energies. New procedures to determine the equilibrium state are derived that in combination with local grid refinement significantly reduce the computational effort and allow for multi-dimensional computations also for more than two components. Artificial parameters in the model as well as numerical threshold values frequently introduced to stabilize the computation are not needed for the extended model. Stability and efficiency of the model and the implementation is verified by means of a spherical symmetric collapse of a laser induced cavitation bubble as well as two-dimensional shock bubble interaction for three-component fluid, where thermal relaxation is performed in the entire flow field.

Keywords: multi-component fluids, non-equilibrium model, phase transition, relaxation process, bubble collapse.
AMS classification: 76Txx, 74Sxx, 76T10.

1   Introduction

Flows of compressible multi-component fluids, where the single components may be in the liquid or the gas phase, respectively, have a wide range of applications. Difficulties in the modeling result from the interaction of the fluids, especially from the exchange of mass and energy across the phase interfaces. Therefore the treatment of the phase interfaces is in the focus of the modeling.

In the literature several models are available that are distinguished in sharp interface and diffuse interface models. A detailed survey of these models can be found in Zein [46]. Here our main interest is on multi-component fluids derived from an ensemble averaging procedure of Drew [12]. A comprehensive introduction to these models can be found in the classical book of Drew and Passman [13].

There are simplified two-phase models available in the literature that can be derived from the above general model by assuming zero relaxation times, see [24]. A detailed discussion of these models is beyond the scope of this work. For this purpose the interested reader is referred to [46] and the references cited therein. Typically reduced models suffer from some short-comings. For instance, conservation of energy might be violated or the system looses its hyperbolicity. Therefore we prefer a full non-equilibrium model, where each component has its own pressure, velocity and temperature and is governed by its own set of fluid equations. For this purpose we consider a general class of non-equilibrium multi-component models that is a generalization of the three-phase model investigated by Hèrard, see Remark 7 in [23].

Obviously, the original two-phase model by Baer and Nunziato [5] is a full non-equilibrium model which was modified by Saurel and Abgrall. The modified model also includes relaxation terms for the pressure and the velocities of the components. By instantaneous relaxation

---

procedures equilibrium values for the pressure and the velocity can be found. Using further relaxation procedures to drive the temperatures and the Gibbs free energies and chemical potentials, respectively, into equilibrium mass transfer between the phases can be modeled, see Saurel et al. [40] or Zein et al. [47]. Typically the relaxation procedures for temperature and mass transfer are based on iterative algorithms that are very much time-consuming, see Zein et al. [48]. Thus multi-dimensional applications are only feasible in acceptable computational time on massive parallel architectures. It was just recently, that Pelanti und Shyue [34] published two-dimensional results that were made possible by modifying the algorithm of the relaxation process. Although they do not give any computational times for their results further improvements seem to be possible. Therefore our main objective is to modify the relaxation models and to design relaxation procedures that allow for more efficient multi-dimensional computations. The efficiency is further improved by combining the discretization of these models with multiresolution-based grid adaptation techniques, see Müller [31, 32].

For the relaxation model we follow the ideas of Zein et al. [48] but improve the modeling in several aspects: (1) First of all, we simplify the relaxation procedures for pressure, temperature and Gibbs free energy, both for two-phase models with two and three components, respectively. (2) Opposite to [48] we avoid the calculation of model parameters that allows us to find the relaxed pressures and temperatures directly *without* performing an iterative procedure. (3) In addition, the modeling of mass transfer between two unpurified phases is improved, see also Pelanti and Shyue [34] who only considered pure phases. (4) Instead of Gibbs free energies we relax the chemical potentials. Therefore we may take into account additional components in the phases by considering the mixture entropy and, thus, the model becomes more accurate. (5) Furthermore, we avoid the artificial definition of an interfacial region. This allows us to model *physical* cavitation, which means that we can start from a pure liquid phase. The vapor phase will be created by expansion. In previous work it was necessary to start with an appreciable amount of vapor, for instance 1% in [47] and also in [34]. Nevertheless in our model we avoid *unphysical* nucleation or *unphysical* cavitation. We will give evidence for this by numerical examples. (6) Another essential difference to [47] is that we do not restrict mass transfer to metastable states with liquid temperature larger than the saturation temperature. Typically, condensation processes are not considered due to this restriction, cf. [47] and [34], whereas our model allows also to deal with these processes. (7) Moreover, we perform thermal relaxation also when no mass transfer occurs. This is physically reasonable. For instance this may happen in gas mixtures. (8) Finally we improve the efficiency of the relaxation procedure where we perform pressure and temperature relaxation simultaneously. By this we avoid the approximate pressure relaxation procedure, see [26] or [46], that may cause numerical instabilities and, thus, very small time steps.

For a physically relevant application we present simulations for laser induced cavitation bubbles. These are motivated by experiments of Lauterborn et al.. An overview on this work can be found in the review article [27]. Recent experiments [41, 44] at elevated water temperatures indicate that the amount of non-condensable gas in the bubble might have a significant influence on the collapse and the rebound of the bubble. In the book of Müller [30], p. 301-312, it is explained that in addition of water vapor at least one further substance must be inside the bubble to guarantee a stable equilibrium state of a surviving bubble. In order to investigate this numerically the original two-component model had to be generalized to a multi-component model.

Motivated by lithotripter shock wave experiments, see [1], we investigate the interaction of a collapsing bubble with a planar shock wave. This is a genuinely two-dimensional problem. Again, we perform computations where the bubble is filled with liquid-vapor and non-condensable gas.

The paper is organized as follows. In Section 2 we introduce the non-equilibrium multi-component model and summarize some of its properties. In Section 3 we discretize the model by an operator splitting. For this purpose, we first apply the Saurel-Abgrall approach for the stable discretization of the homogeneous fluid equations. Then the relaxation terms are relaxed to the equilibrium state. In particular, the thermal and chemical relaxation procedures are given in detail due to its originality. Finally in Section 4 we present numerous numerical results. First of all, real cavitation is investigated by means of one-dimensional computations. Then the influence of the amount of non-condensable gas on the collapse of a vapor-filled

bubble is studied by means of a spherical bubble collapse. We conclude with two-dimensional computations for a shock-bubble interaction.

2   Mathematical formulation of the model

First of all, we describe the full non-equilibrium model and derive from this the mixture model and the equilibrium model, see Section 2.1. To close the model we specify the equations of state, see Section 2.2, and the relaxation terms, see Section 2.3. Finally we summarize some physical and mathematical properties of the different models, see Section 2.4.

2.1   Non-equilibrium multi-component model

For the multi-component model we use the Saurel-Abgrall approach [37] that is derived by the ensemble averaging procedure of Drew [12] and neglecting all dissipative terms everywhere except at the interfaces. It can be considered a modified form of the Baer and Nunziato model [5].

Thus the multi-component flow is described by a non-equilibrium model where all components are present in each point of the space-time continuum. Each component $k = 1, \ldots, K$ has density ρ_k, velocity $\boldsymbol{v}_k$ and pressure p_k, The amount of each component is determined by its volume fraction α_k. The volume fractions are related by the saturation constraint

$$\sum_{k=1}^{K} \alpha_k = 1, \quad \alpha_k \in [0,1]. \tag{1}$$

In analogy to the two-phase model of Saurel and Abgrall [37] the fluid equations for each component can be written as

$$\partial_t (\alpha_k \, \rho_k) + \nabla \cdot (\alpha_k \, \rho_k \, \boldsymbol{v}_k) = S_{\rho,k}, \tag{2}$$

$$\partial_t (\alpha_k \, \rho_k \, \boldsymbol{v}_k) + \nabla \cdot (\alpha_k \, \rho_k \, \boldsymbol{v}_k \, \boldsymbol{v}_k^T + \alpha_k \, p_k \, \boldsymbol{I}) = -\sum_{l=1, \neq k}^{K} P_{k,l} \, \nabla \, \alpha_l + \boldsymbol{S}_{\rho \boldsymbol{v}, k}, \tag{3}$$

$$\partial_t (\alpha_k \, \rho_k \, E_k) + \nabla \cdot (\alpha_k \, \rho_k \, \boldsymbol{v}_k \, (E_k + p_k/\rho_k)) = -\sum_{l=1, \neq k}^{K} P_{k,l} \, \boldsymbol{V}_I \cdot \nabla \, \alpha_l + S_{\rho E, k}, \tag{4}$$

where we neglect effects due to viscosity, heat conduction, surface tension and gravity. Nevertheless, due to the thermal relaxation procedures we account for heat exchange between the components. In our notation $E_k = e_k + \boldsymbol{v}_k^2/2$ is the total specific energy with e_k the specific internal energy of component k. The terms $P_{k,l}$ and $\boldsymbol{V}_I$ are the interfacial pressures and velocity, respectively. The gradient terms on the right-hand side account for the interaction between different components. There may be other contributions to be accounted for, see [13], p. 68 ff and 144 ff. The fluid equations are supplemented by an equation of state

$$p_k = p_k(\rho_k, e_k) \quad \text{resp.} \quad e_k = e_k(\rho_k, p_k) \tag{5}$$

for each of the components, see Section 2.2 for the specific choice. The evolution of the volume fractions is characterized by the non-conservative equations

$$\partial_t \, \alpha_k + \boldsymbol{V}_I \cdot \nabla \, \alpha_k = S_{\alpha,k}, \ k = 1, \ldots, K. \tag{6}$$

Due to the saturation condition (1) we only need $K - 1$ equations. Without loss of generality we express α_K by the other volume fractions, i.e.,

$$\alpha_K = 1 - \sum_{k=1}^{K-1} \alpha_k, \ \nabla \alpha_K = -\sum_{k=1}^{K-1} \nabla \alpha_k, \ S_{\alpha,K} = -\sum_{k=1}^{K-1} S_{\alpha,k}. \tag{7}$$

The source terms $S_{\alpha,k}$, $S_{\rho,k}$, $\boldsymbol{S}_{\rho \boldsymbol{v}, k}$ and $S_{\rho E, k}$ on the right-hand sides of (2), (3), (4) and (6) describe the relaxation process corresponding to mass, momentum and energy transfer between

the different components corresponding to the relaxation of velocity, pressure, temperature and mass, $\xi \in \{v, p, T, \mu\}$, i.e.,

$$S_{\alpha,k} := \sum_\xi S_{\alpha,k}^\xi, \ S_{\rho,k} := \sum_\xi S_{\rho,k}^\xi, \ \boldsymbol{S}_{\rho\boldsymbol{v},k} := \sum_\xi \boldsymbol{S}_{\rho\boldsymbol{v},k}^\xi, \ S_{\rho E,k} := \sum_\xi S_{\rho E,k}^\xi,$$

These depend on the specific components at hand that will be discussed in Section 2.3. In order to ensure conservation of mass, momentum and energy at equilibrium the relaxation terms have to satisfy the conservation constraints

$$\sum_{k=1}^K S_{\alpha,k}^\xi = 0, \quad \sum_{k=1}^K S_{\rho,k}^\xi = 0, \quad \sum_{k=1}^K \boldsymbol{S}_{\rho\boldsymbol{v},k}^\xi = \boldsymbol{0}, \quad \sum_{k=1}^K S_{\rho E,k}^\xi = 0 \tag{8}$$

for each relaxation type $\xi \in \{v, p, T, \mu\}$.

From the non-equilibrium model we can derive the equations for the mixture. For this purpose we introduce the mixture quantities

$$p := \sum_{k=1}^K \alpha_k\, p_k, \ \rho := \sum_{k=1}^K \alpha_k\, \rho_k, \ \rho\boldsymbol{v} := \sum_{k=1}^K \alpha_k\, \rho_k\, \boldsymbol{v}_k, \ \rho E := \sum_{k=1}^K \alpha_k\, \rho_k\, E_k \tag{9}$$

for pressure, density, momentum and total energy, respectively. In order to ensure conservation of mass, momentum and total energy of the mixture we need to impose constraints on the interfacial pressures

$$\sum_{k=1,\neq l}^K P_{k,l} = P_I = const. \quad \forall l = 1, \dots, K. \tag{10}$$

Then by summation of the single-component fluid equations (2), (3), (4) and employing the constraints (1) and (8) we obtain

$$\partial_t\, (\rho) + \nabla \cdot (\rho\, \boldsymbol{v}) = 0, \tag{11}$$

$$\partial_t\, (\rho\, \boldsymbol{v}) + \nabla \cdot (\rho\, \boldsymbol{v}\, \boldsymbol{v}^T + p\, \boldsymbol{I}) = -\nabla \cdot \left(\sum_{k=1}^K \alpha_k\, \rho_k\, (\boldsymbol{v} - \boldsymbol{v}_k)\, (\boldsymbol{v} - \boldsymbol{v}_k)^T \right), \tag{12}$$

$$\partial_t\, (\rho\, E) + \nabla \cdot (\rho\, \boldsymbol{v}\, (E + p/\rho)) = -\nabla \cdot \left(\sum_{k=1}^K \alpha_k\, \rho_k\, (H_k - H)\, (\boldsymbol{v}_k - \boldsymbol{v}) \right). \tag{13}$$

Here the total enthalpy of the single components and the mixture, respectively, are defined as

$$H_k := E_k + \frac{p_k}{\rho_k}, \quad H := \frac{1}{\rho} \sum_{k=1}^K \alpha_k\, \rho_k H_k = E + \frac{p}{\rho}. \tag{14}$$

We note that there are contributions corresponding to the slip between the mixture velocity $\boldsymbol{v}$ and the velocities of the components $\boldsymbol{v}_k$. In the multi-component model of Drew and Passman these terms are added to the mixture stress tensor and the mixture heat flux, see [13], p. 82-83. However, assuming that the velocities are at *equilibrium*, i.e.,

$$\boldsymbol{v} = \boldsymbol{v}_1 = \dots = \boldsymbol{v}_K, \tag{15}$$

then the right-hand sides vanish and we are left with the equilibrium model

$$\partial_t\, \rho + \nabla \cdot (\rho\, \boldsymbol{v}) = 0, \tag{16}$$
$$\partial_t\, (\rho\, \boldsymbol{v}) + \nabla \cdot (\rho\, \boldsymbol{v}\, \boldsymbol{v}^T + p\, \boldsymbol{I}) = \boldsymbol{0}, \tag{17}$$
$$\partial_t\, (\rho\, E) + \nabla \cdot (\rho\, \boldsymbol{v}\, (E + p/\rho)) = 0. \tag{18}$$

It remains to define the interfacial pressures $P_{k,l}$ and the interfacial velocity $\boldsymbol{V}_I$. They have to be chosen in agreement with the 2nd law of thermodynamics. An admissible choice has to satisfy the constraints

$$\sum_{k=1}^K \frac{1}{T_k}(P_{k,l} - p_k)(1 - \delta_{l,k})(\boldsymbol{v}_k - \boldsymbol{V}_I) = \sum_{k=1}^{K-1} \frac{1}{T_k}(P_{k,K} - p_k)(\boldsymbol{v}_k - \boldsymbol{V}_I) \tag{19}$$

for $l = 1, \ldots, K - 1$ in addition to the conservation constraint (10). This ensures that the interfacial pressures and the interfacial velocity do not contribute to the entropy production of the mixture entropy. In [20] it has been proven that for

$$P_I := \sum_{k=2}^{K} p_k, \quad \boldsymbol{V}_I := \boldsymbol{v}_1 \tag{20}$$

there exists a unique choice for $P_{k,l}$ satisfying the constraints (19) and (10). Obviously, in case of pressure equilibrium, i.e., $p_k = const.$, $k = 1, \ldots, K$, we may choose $P_{k,l} = p$. Therefore we will assume that for any admissible choice of $P_{k,l}$ and $\boldsymbol{V}_I$ the interfacial pressures and the interfacial velocity coincide with the equilibrium state, i.e.,

$$P_{k,l} = p \quad \text{and} \quad \boldsymbol{V}_I = \boldsymbol{v}. \tag{21}$$

2.2   Equation of State

Each component is complemented by its own equation of state (EOS) as a pure material. Here we choose the stiffened gas model that was introduced by Harlow and Amsden [22]. It can be considered as a combination of the perfect gas law and the barotropic Tait equation supplemented with an appropriate energy law [42]. The corresponding thermal and caloric EOS read

$$p_k(\rho_k, e_k) = (\gamma_k - 1)\, \rho_k\, (e_k - q_k) - \gamma_k\, \pi_k, \tag{22}$$

$$T_k(\rho_k, e_k) = (e_k - q_k - \pi_k/\rho_k)/c_{v,k}, \tag{23}$$

where T_k is the temperature and the material parameters are the ratio of specific heats γ_k, the specific heat at constant volume $c_{v,k}$, the minimal pressure π_k and the heat of formation q_k. Equivalently, these equations can be rewritten as

$$e_k(\rho_k, p_k) = \frac{p_k + \gamma_k \pi_k}{\rho_k\,(\gamma_k - 1)} + q_k, \tag{24}$$

$$T_k(\rho_k, p_k) = \frac{p_k + \pi_k}{c_{v,k}\,\rho_k\,(\gamma_k - 1)}. \tag{25}$$

From the equation of states we conclude by

$$T_k ds_k = de_k - \frac{p_k}{\rho_k^2} d\rho_k \tag{26}$$

from equilibrium thermodynamics for the specific entropy s_k and the Gibbs free energy g_k

$$s_k(p_k, T_k) = c_{v,k}\, \ln\left(\frac{T_k^{\gamma_k}}{(p_k + \pi_k)^{\gamma_k - 1}}\right) + q'_k, \tag{27}$$

$$g_k(p_k, T_k) = e_k + p_k/\rho_k - T_k s_k. \tag{28}$$

Here q'_k is another material parameter. Furthermore the speed of sound is given by

$$c_k^2 := \left.\frac{\partial p_k}{\partial \rho_k}\right|_{s_k = const} = \frac{p_k}{\rho_k^2} \left.\frac{\partial p_k}{\partial e_k}\right|_{\rho_k = const} + \left.\frac{\partial p_k}{\partial \rho_k}\right|_{e_k = const} = \frac{(p_k + \pi_k)\gamma_k}{\rho_k}. \tag{29}$$

Note that the stiffened gas EOS allows for negative pressures while $p_k + \pi_k$ remains positive, i.e., the system is hyperbolic.

In particular, we are interested in the three-component model, i.e., $K = 3$, with water vapor ($k = 1$), liquid water ($k = 2$) and inert gas ($k = 3$). The corresponding material parameters are listed in Table 1. To model the chemical relaxation process we need the chemical potentials of the vapor and the liquid phase. In this model the gas phase is a mixture of water vapor and some other constituent, where all phases are modeled as an ideal gas. Then the chemical potential of the vapor phase is given by

$$\mu_1 = g_1 + \frac{\kappa_b T}{m_{01}} \ln\left(\frac{\alpha_1}{\alpha_1 + \alpha_3}\right). \tag{30}$$

phase	γ	π [Pa]	c_v [J/kg/K]	q [J/kg]	q' [J/kg/K]
vapor (1)	1.327	0	1200	1.995000×10^6	2.410×10^3
water (2)	2.057	1.066×10^9	3449	-1.994674×10^6	3.578×10^4
gas (3)	1.4	0	10100	0	0

Table 1: Material parameters taken from [46].

Here κ_b denotes the Boltzmann constant and m_{01} is the mass of a single water molecule. Note that we only sum over the gas phase components. In the special case of vanishing third component, i.e., $\alpha_3 = 0$, the chemical potential of the vapor phase reduces to the vapor Gibbs free energy. The chemical potential μ_2 of the liquid phase equals its Gibbs free energy g_2, i.e.,

$$\mu_2 = g_2 \,.$$

In chemical equilibrium the chemical potentials of the vapor and the liquid phase equal each other. For details see the book of Müller and Müller [30], Section 8.2.4.

2.3 Relaxation terms

The non-equilibrium model presented in Section 2.1 allows for different values for velocities, pressures, temperatures as well as chemical potentials at the same point. Therefore one has to introduce a relaxation mechanism, that drives all these quantities into equilibrium. Typically it is distinguished between mechanical and thermal relaxation processes that relax either pressures and velocities or temperatures and chemical potentials to equilibrium.

Mechanical relaxation. The *pressure relaxation* implies volume variations that induce energy variations due to the interfacial pressure work. Here we extend the pressure relaxation vector given in [37] for a two-phase model according to [46] by introducing a pressure average that we choose as the mixture pressure. The pressure relaxation terms then read

$$S_{\alpha,k}^p := \theta_p \, \alpha_k \, (p_k - p), \ S_{\rho,k}^p := 0, \ \boldsymbol{S}_{\rho\boldsymbol{v},k}^p := \boldsymbol{0}, \ S_{\rho E,k}^p := \theta_p \, \alpha_k \, p(p - p_k). \tag{31}$$

Here θ_p denotes the pressure relaxation parameter. Similarly the *velocity relaxation* terms read

$$S_{\alpha,k}^v = S_{\rho,k}^v := 0, \ \boldsymbol{S}_{\rho\boldsymbol{v},k}^v := \theta_v \, \alpha_k \, \rho_k \, (\boldsymbol{v} - \boldsymbol{v}_k), \ S_{\rho E,k}^v := \theta_v \, \alpha_k \, \rho_k \, \boldsymbol{v} \cdot (\boldsymbol{v} - \boldsymbol{v}_k) \tag{32}$$

with the velocity relaxation parameter θ_v. Performing velocity and pressure relaxation the fluid mixture is in mechanical equilibrium, i.e., $p_k = p^\infty$ and $\boldsymbol{v}_k = \boldsymbol{v}^\infty$, $k = 1, \dots, K$. Note that by the definition of the mixture velocity and mixture pressure (9) the conservation constraints (8) are satisfied. For more details on mechanical relaxation see Baer and Nunziato [5] or Baer [15] for two-phase models.

Thermal relaxation. For the modeling of *temperature relaxation* we follow Zein [46] and introduce the temperature relaxation parameter θ_T and the corresponding relaxation terms

$$S_{\alpha,k}^T := \frac{\theta_T}{\kappa_k} \, \alpha_k \, (\hat{T} - T_k), \ S_{\rho,k}^T := 0, \ \boldsymbol{S}_{\rho\boldsymbol{v},k}^T := \boldsymbol{0}, \ S_{\rho E,k}^T := \theta_T \, \alpha_k \, (\hat{T} - T_k), \tag{33}$$

where the mean of the temperature is defined as the mixture temperature

$$\hat{T} := \sum_{k=1}^K \alpha_k \, T_k.$$

Note that by the definition of $\hat{T}$ the conservation constraints (8) are satisfied and at temperature equilibrium, i.e., $T_k = T^\infty$, $k = 1, \dots, K$, it coincides with the equilibrium temperature, i.e., $\hat{T} = T^\infty$. The relaxation parameters κ_k are introduced in Zein [46] and Zein et al. [47] in case of a two-phase and a three-phase model, respectively, to ensure the pressure keeping equilibrium during the temperature relaxation.

However, in our new thermal relaxation approach these parameters do not enter explicitly the computation of the equilibrium state, cf. [34] and, thus, is not given here.

Chemical potential relaxation. Mass transfer between different phases of the same substance occurs, whenever these phases are not in thermal equilibrium. This physical fact is the key idea to model the mass transfer by relaxation of the chemical potentials. It is obvious, that from now on it is necessary to identify the phases. The gas phase is assumed to be a mixture of water vapor and some further gas. Here we only consider three components, i.e., $K = 3$, with water vapor ($k = 1$), liquid water ($k = 2$) and inert gas ($k = 3$). Thermal equilibrium is achieved, if the chemical potential of the water vapor phase equals the Gibbs free energy of the liquid water phase. In the limit case of no inert gas the expression of the chemical potential of the water vapor phase reduces to the Gibbs free energy, see (30). The mass flux $\dot{m}$ between the liquid and the vapor phase is driven by the difference of their chemical potentials, i.e., $\dot{m} = \dot{m}(\mu_1 - \mu_2)$. In particular, the mass flux vanishes if and only if the difference of the chemical potentials is zero, i.e., $\mu_1 = \mu_2$.

The relaxation terms of chemical potentials are given by

$$S_{\alpha,1}^\mu := \theta_\mu \, \frac{\dot{m}}{\varrho_1}, \; S_{\rho,1}^\mu := \theta_\mu \, \dot{m}, \; \boldsymbol{S}_{\rho\boldsymbol{v},1}^\mu := \theta_\mu \, \dot{m} \, \boldsymbol{V}_I, \; S_{\rho E,1}^\mu := \theta_\mu \, \dot{m} \left(\epsilon_1 + \frac{\boldsymbol{V}_I^2}{2} \right),$$

$$S_{\alpha,2}^\mu := \theta_\mu \, \frac{\dot{m}}{\varrho_2}, \; S_{\rho,2}^\mu := -\theta_\mu \, \dot{m}, \; \boldsymbol{S}_{\rho\boldsymbol{v},2}^\mu := -\theta_\mu \, \dot{m} \, \boldsymbol{V}_I, \; S_{\rho E,2}^\mu := -\theta_\mu \, \dot{m} \left(\epsilon_2 + \frac{\boldsymbol{V}_I^2}{2} \right),$$

$$S_{\alpha,3}^\mu := -\theta_\mu \, \dot{m} \left(\frac{1}{\varrho_1} + \frac{1}{\varrho_2} \right), \; S_{\rho,3}^\mu := 0, \; \boldsymbol{S}_{\rho\boldsymbol{v},3}^\mu := \boldsymbol{0}, \; S_{\rho E,3}^\mu := \theta_\mu \, \dot{m} \, (\epsilon_2 - \epsilon_1), \qquad (34)$$

with the relaxation parameter θ_μ. Formulas for the parameters $\varrho_1, \varrho_2, \epsilon_1, \epsilon_2$ can be found in [46, 48]. For details on the physics see the book of Müller and Müller [30].

The relaxation terms (31), (32), (33), (34) are of major importance when dealing with interface problems, see for instance Saurel and Abgrall [37] or Lallemand and Saurel [26] for mechanical relaxation terms. Typically, it is assumed that pressure and velocity relax instantaneously, see [37], whereas the thermal relaxation and the relaxation of chemical potentials are much slower, see Zein [46]. Here we are interested only in the equilibrium state that is characterized by vanishing relaxation terms rather than the transient relaxation process itself. Since the equilibrium state does not depend on the order of relaxation, the relaxation parameters θ_ξ, $\xi \in \{p, v, T, \mu\}$, drop out and have not to be known explicitly.

As will be explained later on in Section 3.3 in our new procedure to determine the temperature equilibrium state and the mass equilibrium state the parameters κ_k and ε_k, ϱ_k, $k = 1, 2$, respectively, do not enter explicitly and, thus, are not given here. This is an important improvement to the modeling proposed in [46, 48], since we avoid an additional iteration process in the relaxation procedure.

Furthermore, our modeling of the mass equilibrium state is much more physical than the one presented in [46, 48] by taking into account chemical potentials instead of Gibbs free energies. In [46, 48] the Gibbs free energy is relaxed, which neglects the effect of mixture entropy in cases of impure substances. The expression for the chemical potential is based on the assumption that the vapor phase is modeled as an ideal gas.

2.4 Properties of the non-equilibrium model, the mixture model and the equilibrium model

Here we will briefly summarize some physical and mathematical properties of the non-equilibrium model (2), (3), (4), (6), the mixture model (11), (12), (13) and the equilibrium model (16), (17), (18). Details on the proofs can be found in [20].

Conservation property: Due to the interaction terms corresponding to the gradients of the volume fractions on the right-hand side of the non-equilibrium model the system cannot be written in divergence form and, thus, momentum and energy are not conserved. However, thanks to the conservation constraints (8) and the saturation condition (1) these terms vanish in the mixture model and the equilibrium model, respectively. Hence, mass, momentum and energy are conserved in these models. Note that in our computations we are interested only in the equilibrium state.

Hyperbolicity and subcharacteristic condition: Neglecting the relaxation terms in the non-equilibrium model it can be proven that the system is non-strictly hyperbolic, if the

non-resonance condition

$$(\boldsymbol{v}_k \cdot \boldsymbol{n} - \boldsymbol{V}_I \cdot \boldsymbol{n})^2 \neq c_k^2 \quad \text{and} \quad \alpha_k \neq 0 \qquad \forall\, k = 1, \ldots, K$$

holds. In particular, the eigenvalues corresponding to the quasi-conservative non-equilibrium system for α_k, $k = 1, \ldots, K-1$, and $(\rho_k, \boldsymbol{v}_k, p_k)$, $k = 1, \ldots, K$, in normal direction $\boldsymbol{n}$ are

$$\begin{align}
\lambda_{I,k} &= \boldsymbol{V}_I \cdot \boldsymbol{n},\ k = 1, \ldots, K-1, & (35) \\
\lambda_{k,i} &= \boldsymbol{v}_k \cdot \boldsymbol{n},\ k = 1, \ldots, K,\ i = 1, \ldots, d, & (36) \\
\lambda_{k,\pm} &= \boldsymbol{v}_k \cdot \boldsymbol{n} \pm c_k,\ k = 1, \ldots, K, & (37)
\end{align}$$

where c_k is the sound speed (29) corresponding to component k. Similarly, the equilibrium model is hyperbolic. In particular, the eigenvalues of the quasi-conservative equilibrium system for $(\rho, \boldsymbol{v}, \rho E)$ in normal direction $\boldsymbol{n}$ are determined by

$$\lambda_{\pm} = \boldsymbol{v} \cdot \boldsymbol{n} \pm c, \quad \lambda_i = \boldsymbol{v} \cdot \boldsymbol{n},\ i = 1, \ldots, d, \tag{38}$$

where the mixture sound speed is defined as

$$\rho\, c^2 := \sum_{k=1}^{K} \alpha_k \rho_k\, c_k^2. \tag{39}$$

By the definition of the mixture velocity, the mixture density (9) and the mixture sound speed (39) we observe that these eigenvalues are related to the eigenvalues (35) of the non-equilibrium model in the following way:

$$\lambda_{\pm} \in \left[\min_{k=1,\ldots,K} \lambda_{k,\pm},\ \max_{k=1,\ldots,K} \lambda_{k,\pm} \right],$$

$$\lambda_i \in \left[\min\left(\min_{k=1,\ldots,K-1} \lambda_{I,k},\ \min_{k=1,\ldots,K} \lambda_{k,i} \right),\ \max\left(\max_{k=1,\ldots,K-1} \lambda_{I,k},\ \max_{k=1,\ldots,K} \lambda_{k,i} \right) \right],$$

for $i = 1, \ldots, d$. Here the eigenvalues of both the non-equilibrium and the equilibrium system are evaluated at *equilibrium* states. Thus the so-called sub-characteristic condition first introduced by Liu [28] holds true. This ensures stability in the limit of vanishing relaxation terms, i.e., $\theta_\xi \to \infty$. Note that similar results have been proven recently by Flåtten and Lund [16] for a hierarchy of two-phase relaxation models.

Frame indifference: Since the results of an experiment should be independent of the observer's position a physical meaningful model should reflect this behavior. This property is referred to as frame indifference in the literature, cf. [13], p. 31 ff, i.e., performing the change of frame

$$t^* = t + a, \quad \boldsymbol{x}^* = \boldsymbol{x}_0^*(t) + \boldsymbol{Q}(t)(\boldsymbol{x} - \boldsymbol{x}_0), \tag{40}$$

with constant values a and $\boldsymbol{x}_0$ and $\boldsymbol{Q}$ an orthogonal matrix, then a scalar f, a vector $\boldsymbol{u}$ and a tensor $\boldsymbol{T}$ are called objective, if

$$f^*(t^*, \boldsymbol{x}^*) = f(t, x), \ \boldsymbol{u}^*(t^*, \boldsymbol{x}^*) = \boldsymbol{Q}(t)\boldsymbol{u}(t, x), \ \boldsymbol{T}^*(t^*, \boldsymbol{x}^*) = \boldsymbol{Q}(t)\boldsymbol{T}(t, x)\boldsymbol{Q}^T(t).$$

It is well-known that the fluid equations for a single phase are not invariant under a general Euclidean change of frame but under a Galilean transformation where we choose $\dot{\boldsymbol{x}}_0 = 0$, $\dot{\boldsymbol{Q}} = \boldsymbol{0}$ or, equivalently, $\boldsymbol{Q} = const$, $\boldsymbol{x}_0^*(t) = \boldsymbol{c}_0 + \boldsymbol{c}_1 t$, $\boldsymbol{c}_1, \boldsymbol{c}_2 = const$ in (40). To ensure Galilean invariance of the non-equilibrium model, the following relations have to hold true for the relaxation terms

$$\begin{align}
S_{\alpha^*,k}^* &:= S_{\alpha,k} = S_{\alpha^*,k}, \\
S_{\rho^*,k}^* &:= S_{\rho,k} = S_{\rho^*,k}, \\
\boldsymbol{S}_{(\rho\boldsymbol{v})^*,k}^* &:= S_{\rho,k}\dot{\boldsymbol{x}}_0^* + \boldsymbol{Q}\boldsymbol{S}_{\rho\boldsymbol{v},k} = \boldsymbol{S}_{(\rho\boldsymbol{v})^*,k}, \\
S_{(\rho E)^*,k}^* &:= S_{(\rho E),k} + (\boldsymbol{Q}\boldsymbol{S}_{\rho\boldsymbol{v},k} + S_{\rho,k}\dot{\boldsymbol{x}}_0^*) \cdot \boldsymbol{x}_0^* - 0.5(\dot{\boldsymbol{x}}_0^*)^2 S_{\rho,k} = S_{(\rho E)^*,k}.
\end{align}$$

These are satisfied for the relaxation terms introduced in Section 2.3. Since the mixture model and the equilibrium model are derived from the non-equilibrium model by summation these models are also Galilean invariant.

Entropy and 2nd law of thermodynamics: A physically meaningful model has to satisfy the principles of thermodynamics. From the relation (26) resulting from equilibrium thermodynamics we derive for the non-equilibrium model the entropy equation of component k

$$\partial_t \left(\alpha_k \rho_k s_k \right) + \nabla \cdot \left(\alpha_k \rho_k s_k \boldsymbol{v}_k \right) = \Pi_k + S_{\rho s,k}$$

with the production terms due to interfacial quantities and relaxation terms

$$\Pi_k \quad := \quad \frac{1}{T_k} \sum_{l=1, \neq k}^{K} \left(P_{k,l} - p_k \right) \cdot \left(\boldsymbol{v}_k - \boldsymbol{V}_I \right) \cdot \nabla \alpha_l, \tag{41}$$

$$S_{\rho s,k} \quad := \quad \frac{1}{T_k} \left(p_k S_{\alpha,k} + (u_k - g_k) S_{\rho,k} - \boldsymbol{v}_k \cdot \boldsymbol{S}_{\rho \boldsymbol{v},k} + S_{\rho E,k} \right). \tag{42}$$

Introducing the entropy of the mixture $\rho s := \sum_{k=1}^{K} \alpha_k \rho_k s_k$ the entropy law of the mixture reads

$$\partial_t \left(\rho s \right) + \nabla \cdot \left(\rho s \boldsymbol{v} \right) = -\nabla \cdot \left(\sum_{k=1}^{K} \alpha_k \rho_k s_k (\boldsymbol{v}_k - \boldsymbol{v}) \right) + \sum_{k=1}^{K} (\Pi_k + S_{\rho s,k}). \tag{43}$$

Note that $-\rho s$ is a convex function of the volume fractions α_k, $k = 1, \ldots, K-1$ and the conserved quantities $(\alpha_k \rho_k, \alpha_k \rho_k \boldsymbol{v}_k, \alpha_k \rho_k E_k)$, $k = 1, \ldots, K$ provided that the energies e_k are convex functions of the specific volume $\tau_k = 1/\rho_k$ and entropy s_k, i.e., in case of thermodynamical stability. In view of the 2nd law of thermodynamics we have to ensure that the sums $\Pi := \sum_{k=1}^{K} \Pi_k$ and $S_{\rho s} := \sum_{k=1}^{K} S_{\rho s,k}$ are non-negative. This provides us with admissible closing conditions for the interfacial pressures and interfacial velocity as well as the relaxation terms. Obviously, the sign of Π cannot be controlled. Therefore this term must drop out. For instance, this holds true for (20) where the interfacial pressures $P_{k,l}$ have to be appropriately chosen, see [20]. For a two-component fluid, another alternative is given in [17] that has been proven in [36] to cancel this term. For the entropy production terms due to mechanical relaxation we determine for the relaxation terms (31) and (32)

$$S_{\rho s}^{v} = \sum_{k=1}^{K} \theta_v \frac{\alpha_k \rho_k}{T_k} (\boldsymbol{v} - \boldsymbol{v}_k)^2 \geq 0, \quad S_{\rho s}^{p} = \sum_{k=1}^{K} \theta_p \frac{\alpha_k}{T_k} (p - p_k)^2 \geq 0. \tag{44}$$

For the thermal relaxation we obtain for the relaxation term (33)

$$S_{\rho s}^{T} = \theta_T \sum_{k=1}^{K} \frac{1}{T_k} \alpha_k (\hat{T} - T_k) \left(\frac{p_k}{\kappa} + 1 \right). \tag{45}$$

This term can be proven to be non-negative only if the pressures are in equilibrium, see also [46]. Finally, we derive for the entropy production due chemical relaxation

$$S_{\rho s}^{\mu} = \theta_\mu \frac{\dot{m}}{T} (g_2 - g_1) = \frac{\theta_\mu \dot{m}}{T} (g_2 - \mu_1) + \frac{\theta_\mu \dot{m}}{T} \frac{\kappa_b T}{m_{01}} \ln \frac{\alpha_1}{1 - \alpha_2} \tag{46}$$

assuming mechanical and thermal equilibrium.

$$\sum_{k=1}^{3} S_{\rho s,k}^{\mu} = \frac{\theta_\mu \dot{m}}{T} (g_2 - g_1) = \frac{\theta_\mu \dot{m}}{T} (g_2 - \mu_1) + \frac{\theta_\mu \dot{m}}{T} \frac{\kappa_b T}{m_{01}} \ln \frac{\alpha_1}{1 - \alpha_2}$$

Since that $\dot{m}$ is proportional to the difference of the chemical potentials $\mu_2 - \mu_1$ describing the change of mass of the water vapor. Therefore the first term is non-negative whereas the second term is proportional to $-\dot{m}$. Note that one would obtain a non-negative term when accounting for the mixing in the entropy, i.e.,

$$\rho s = \sum_{k=1}^{3} \alpha_k \rho_k s_k - \alpha_1 \rho_1 \frac{\kappa_b}{m_{01}} \ln \frac{\alpha_1}{\alpha_1 + \alpha_3} - \alpha_3 \rho_3 \frac{\kappa_b}{m_{03}} \ln \frac{\alpha_3}{\alpha_1 + \alpha_3}.$$

3 Discretization

For a condensed presentation of the discretization it is convenient to rewrite the system (2), (3), (4) and (6) in matrix-vector representation

$$\partial_t \, \alpha_k + \boldsymbol{V}_I \cdot \nabla \, \alpha_k = S_{\alpha,k}(\boldsymbol{w}), \; k = 1, \ldots, K-1, \tag{47}$$

$$\partial_t \, \boldsymbol{u}_k + \nabla \cdot \left(\boldsymbol{f}_k(\alpha_k, \boldsymbol{u}_k) \right) = -\sum_{l=1, \neq k}^{K} \boldsymbol{H}_{k,l}(\boldsymbol{w}) \, \nabla \, \alpha_l + \boldsymbol{S}_{\boldsymbol{u},k}(\boldsymbol{w}), \; k = 1, \ldots, K, \tag{48}$$

where we make use of the convention (7). This forms a coupled system for the volume fractions $\boldsymbol{\alpha} := (\alpha_1, \ldots, \alpha_{K-1})^T$ and the vectors $\boldsymbol{u}_k$ of the conserved quantities of phase $k = 1, \ldots, K$. These are condensed in the vector $\boldsymbol{w} := (\boldsymbol{\alpha}^T, \boldsymbol{u}_1^T, \ldots, \boldsymbol{u}_K^T)^T$, where the field $\boldsymbol{f}_k := (\boldsymbol{f}_{k,1}, \ldots, \boldsymbol{f}_{k,d})$ of the fluxes in the *ith* coordinate direction and the vector of relaxation terms $\boldsymbol{S}_{\boldsymbol{u},k}$ corresponding to $\boldsymbol{u}_k$ as well as the matrices $\boldsymbol{H}$ are defined by

$$\boldsymbol{u}_k := \begin{pmatrix} \alpha_k \, \rho_k \\ \alpha_k \, \rho_k \, \boldsymbol{v}_k \\ \alpha_k \, \rho_k \, E_k \end{pmatrix}, \; \boldsymbol{f}_{k,i} := \begin{pmatrix} \alpha_k \, \rho_k v_{k,i} \\ \alpha_k \, \rho_k v_{k,i} \, \boldsymbol{v}_k + \alpha_k \, p_k \boldsymbol{e}_i \\ \alpha_k \, \rho_k v_{k,i} \left(E_k + p_k / \rho_k \right) \end{pmatrix}, \tag{49}$$

$$\boldsymbol{H}_{k,l} := \begin{pmatrix} \boldsymbol{0}^T \\ P_{k,l} \boldsymbol{I}_{d \times d} \\ P_{k,l} \boldsymbol{V}_I^T \end{pmatrix}, \; \boldsymbol{S}_{\boldsymbol{u},k} := \begin{pmatrix} S_{\rho,k} \\ \boldsymbol{S}_{\rho\boldsymbol{v},k} \\ S_{\rho E,k} \end{pmatrix}. \tag{50}$$

Here $\boldsymbol{e}_i \in \mathbb{R}^d$ and $\boldsymbol{I}_{d \times d} \in \mathbb{R}^{d \times d}$ denote the *ith* unit vector and the identity matrix in $\mathbb{R}^d$ and $\mathbb{R}^{d \times d}$, respectively. Note that in case of constant interfacial pressures $P_{k,l} = p$ it holds

$$-\sum_{l=1, \neq k}^{K} \boldsymbol{H}_{k,l}(\boldsymbol{w}) \, \nabla \, \alpha_l = \boldsymbol{H}(\boldsymbol{w}) \, \nabla \, \alpha_k \quad \text{with} \quad \boldsymbol{H} := \begin{pmatrix} \boldsymbol{0}^T \\ p\boldsymbol{I}_{d \times d} \\ p\boldsymbol{V}_I^T \end{pmatrix} \tag{51}$$

due to the saturation constraint (1).

Because of the constraints (10) and (19) on the interfacial pressures $P_{k,l}$ and the interfacial velocity $\boldsymbol{V}_I$, the fluid equations of *all* phases are coupled, i.e., $P_{k,l} = P_{k,l}(\boldsymbol{w})$, $\boldsymbol{V}_I = \boldsymbol{V}_I(\boldsymbol{w})$, whereas the left-hand side of (48) only depends on $\boldsymbol{w}_k := (\alpha_k, \boldsymbol{u}_k^T)^T$. Again note that for $k = K$ we make use of the convention (7).

Following [37] we do not discretize the coupled system (47) and (48) but perform an operator splitting according to Godunov or Strang, see [43, 45], resulting in the system of equations of fluid motion

$$\partial_t \, \alpha_k + \boldsymbol{V}_I \cdot \nabla \, \alpha_k = \boldsymbol{0}, \; k = 1, \ldots, K-1, \tag{52}$$

$$\partial_t \, \boldsymbol{u}_k + \nabla \cdot \left(\boldsymbol{f}_k(\alpha_k, \boldsymbol{u}_k) \right) = -\sum_{l=1, \neq k}^{K} \boldsymbol{H}_{k,l}(\boldsymbol{w}) \, \nabla \, \alpha_l, \; k = 1, \ldots, K, \tag{53}$$

and the system of relaxation

$$\frac{d \, \alpha_k}{d \, t} = S_{\alpha,k}(\boldsymbol{w}), \; k = 1, \ldots, K-1, \tag{54}$$

$$\frac{d \, \boldsymbol{u}_k}{d \, t} = \boldsymbol{S}_{\boldsymbol{u},k}(\boldsymbol{w}), \; k = 1, \ldots, K. \tag{55}$$

Note that the differential equation (52), (53) describes a variation in time and space, whereas the system (54), (55) is an evolution in time only although the state $\boldsymbol{w}$ depends on both time and space. Therefore we use different symbols for the differentiation.

In each time step we thus perform alternately the evolution of the fluid and the relaxation process. The discretization of these two subsystems are discussed below in Sections 3.1 and 3.3.

In order to use the multi-component model also in absence of one or several components, the fluid must be modeled as a mixture of *all* components in the *entire* computational domain. Therefore the fluid contains at least a negligible amount of each fluid. Thus we require $\alpha_k \geq \varepsilon$

for the initial data. This is common practice, see for instance [3, 26, 37, 7]. In [7] ε is chosen to be 10^{-6}, in [3] $\varepsilon = 10^{-8}$. In our computation we mostly choose $\varepsilon = 10^{-8}$. For more details see Section 3.3.5.

During the computation α_k may become smaller. In that case α_k often is set to ε. However, this leads to the violation of conservation of mass, momentum and energy. We avoid this by allowing smaller values for α_k. To guarantee that α_k always stays positive, we terminate the computation whenever α_k drops below a tolerance value of 10^{-18} that never happened in our computations.

3.1 Fluid Discretization: Saurel-Abgrall Approach

The fluid equations (53) are discretized by a finite volume scheme. However, due to the non-conservative term on the right-hand side it is linked to the discretization of the non-conservative evolution equation (52) for the volume fractions. In order to avoid oscillations in the pressures and velocities at the phase interface Saurel and Abgrall [37] suggest to use a special upwind discretization of (52) that preserves homogeneous pressure and velocity fields. Let be $\{V_i\}_i$ the spatial discretization of the computational domain $\Omega \subset \mathbb{R}^d$ and $\{t_n\}_{n\geq 0}$ the temporal discretization which for ease of representation is assumed to be uniform, i.e., $t_{n+1} = t_n + \Delta t$. Then the resulting scheme reads

$$(\alpha_k)_i^{n+1} = (\alpha_k)_i^n - \frac{\Delta t}{|V_i|} \sum_{j \in \mathcal{N}(i)} |\Gamma_{ij}| \, (\overline{\boldsymbol{V}}_I)_{ij} \cdot (\nabla \alpha_k)_{ij}^n, \tag{56}$$

$$(\boldsymbol{u}_k)_i^{n+1} = (\boldsymbol{u}_k)_i^n - \frac{\Delta t}{|V_i|} \sum_{j \in \mathcal{N}(i)} |\Gamma_{ij}| \, \boldsymbol{G}_{ij}^n, \tag{57}$$

where the fluxes $\boldsymbol{G}_{ij}^n$ and the gradients of the volume fractions in normal direction are determined by

$$\boldsymbol{G}_{ij}^n := \boldsymbol{F}_k(\boldsymbol{w}_{ij}^n, \boldsymbol{w}_{ji}^n, \boldsymbol{n}_{ij}) + \sum_{l=1, \neq k}^{K} \boldsymbol{H}_{k,l}(\overline{\boldsymbol{w}}_{ij})(\nabla \alpha_l)_{ij}^n, \tag{58}$$

$$(\nabla \alpha_l)_{ij}^n := ((\overline{\alpha}_l)_{ij} - (\alpha_l)_i^n) \, \boldsymbol{n}_{ij}. \tag{59}$$

Here the quantities $(\overline{\alpha}_l)_{ij}$, $(\overline{\boldsymbol{V}}_I)_{ij}$ and $\overline{\boldsymbol{w}}_{ij}$ are determined by the solution of a Riemann problem at the cell interface Γ_{ij} evaluated from the interior of the cell V_i. For details on the derivation we refer to Appendix A. In case of mechanical equilibrium, the right-hand side in (58) simplifies to

$$\boldsymbol{G}_{ij}^n = \boldsymbol{F}_k(\boldsymbol{w}_{ij}^n, \boldsymbol{w}_{ji}^n, \boldsymbol{n}_{ij}) - \boldsymbol{H}(\overline{\boldsymbol{w}}_{ij})(\nabla \alpha_k)_{ij}^n \tag{60}$$

because of (51). At each cell interface Γ_{ij} of cell V_i with a neighbor cell V_j, $j \in \mathcal{N}(i)$, a numerical flux in outer normal direction $\boldsymbol{n}_{ij}$ to the cell interface is computed in two steps:

(i) In each of the two neighboring cells a quasi-one-dimensional $2nd$ order ENO reconstruction of the primitive variables $(\rho_k, \boldsymbol{v}_k, p_k)$ with van Leer limiter and the volume fractions α_k is computed for *all* components to determine two states $\boldsymbol{w}_{ij}^n$, $\boldsymbol{w}_{ji}^n$ left and right of the cell interface. Note that for the volume fractions we switch to $1st$ order reconstruction whenever the higher order reconstruction of the volume fractions lies outside a tolerance range $[\alpha_{Tol}, 1 - \alpha_{Tol}]$ with $\alpha_{Tol} = 10^{-18}$ in our computations.

(ii) A multi-phase multi-component Riemann problem determined by $\boldsymbol{w}_{ij}^n$, $\boldsymbol{w}_{ji}^n$ is approximately solved using an HLLC-type Riemann solver, see Section 3.2, providing us with an intermediate state $\overline{\boldsymbol{w}} := (\overline{\boldsymbol{\alpha}}^T, \overline{\boldsymbol{u}}_1^T, \ldots, \overline{\boldsymbol{u}}_k^T)^T$ at the cell interface by which we evaluate the flux at the cell interface in normal direction $\boldsymbol{n}$, i.e,

$$\boldsymbol{F}_k(\boldsymbol{w}_{ij}^n, \boldsymbol{w}_{ji}^n, \boldsymbol{n}_{ij}) := \sum_{l=1}^{d} \boldsymbol{f}_{k,l}(\overline{\boldsymbol{w}}(\boldsymbol{w}_{ij}^n, \boldsymbol{w}_{ji}^n)) \, (\boldsymbol{n}_{ij})_l. \tag{61}$$

Note that the intermediate state also enters the approximation (56) of the volume fractions and their gradients (59). In principle, any numerical flux is admissible that is consistent

with the flux, i.e.,

$$\boldsymbol{F}_k(\boldsymbol{w},\boldsymbol{w},\boldsymbol{n}) = \sum_{i=1}^{d} \boldsymbol{f}_{k,i}(\alpha_k, \boldsymbol{u}_k)\, n_i, \ \forall\, \boldsymbol{w} = (\boldsymbol{\alpha}^T, \boldsymbol{u}_1^T, \dots, \boldsymbol{u}_K^T)^T, \tag{62}$$

$$\sum_{j\in\mathcal{N}(i)} |\Gamma_{ij}|\, \boldsymbol{n}_{ij} = \boldsymbol{0}. \tag{63}$$

3.2 HLLC-type Riemann solver

The numerical flux $\boldsymbol{F}_k$ in (58) is determined by approximately solving a Riemann problem for the fluid equations for mass, momentum and energy of *all* pure components, where the volume fractions are considered to be frozen. For this purpose we employ an HLLC-type Riemann solver

$$\boldsymbol{F}_k(\boldsymbol{w}_L, \boldsymbol{w}_R, \boldsymbol{n}) := \begin{cases} \boldsymbol{f}_{k,n}(\boldsymbol{w}_L), & 0 \leq s_L \\ \boldsymbol{f}_{k,n}(\boldsymbol{w}_{L*}) = \boldsymbol{f}_{k,n}(\boldsymbol{w}_L) + s_L(\boldsymbol{u}_{k,*L} - \boldsymbol{u}_{k,L}), & s_L \leq 0 \leq s_* \\ \boldsymbol{f}_{k,n}(\boldsymbol{w}_{R*}) = \boldsymbol{f}_{k,n}(\boldsymbol{w}_R) + s_R(\boldsymbol{u}_{k,*R} - \boldsymbol{u}_{k,R}), & s_* \leq 0 \leq s_R \\ \boldsymbol{f}_{k,n}(\boldsymbol{w}_R), & 0 \geq s_R \end{cases} \tag{64}$$

where "L" and "R" refer to the left and right states at the cell interface, respectively, which is characterized by its normal $\boldsymbol{n}$. The flux normal to the interface is defined by $\boldsymbol{f}_{k,n} := \sum_{i=1}^{d} \boldsymbol{f}_{k,i}\, n_i$.

Following Toro [45] for a single component the intermediate states corresponding to $C \in \{L, R\}$ can be determined as

$$\begin{pmatrix} \alpha_k\,\rho_k \\ \alpha_k\,\rho_k\,\boldsymbol{v}_k \\ \alpha_k\,\rho_k\,E_k \end{pmatrix}_{C*} = \tag{65}$$

$$(\alpha_k\,\rho_k)_C\, \frac{s_C - v_{k,n,C}}{s_C - v_{k,n,*}} \begin{pmatrix} 1 \\ \boldsymbol{v}_{k,C} + (v_{k,n,*} - v_{k,n,C})\,\boldsymbol{n} \\ E_{k,C} + (v_{k,n,*} - v_{k,n,C}) \left(v_{k,n,*} + \frac{p_{k,C}}{\rho_{k,C}\,(s_K - v_{k,n,C})} \right) \end{pmatrix}$$

with normal velocity $v_{k,n} := \boldsymbol{v}_k \cdot \boldsymbol{n}$. For the wave speeds s_L and s_R we follow Davis [11]

$$s_L := \min_{k=1,\dots,K} \{ v_{k,n,L} - c_{k,L}, v_{k,n,R} - c_{k,R} \}, \tag{66}$$

$$s_R := \max_{k=1,\dots,K} \{ v_{k,n,L} + c_{k,L}, v_{k,n,R} + c_{k,R} \}. \tag{67}$$

In case of a multiphase fluid the wave speed s_* turns out to be

$$s_* = v_{n,*} = \frac{p_L - p_R - \rho_L\, v_{n,L}\,(s_L - v_{n,L}) + \rho_R\, v_{n,R}\,(s_R - v_{n,R})}{\rho_R\,(s_R - v_{n,R}) - \rho_L\,(s_L - v_{n,L})}. \tag{68}$$

Opposite to [45], we use here the mixture values for pressure, velocity and density defined by (9), where we employ velocity and pressure equilibrium. Note that (68) becomes an approximation of the exact wave speed s_* if the left and right states are not in mechanical equilibrium. A detailed derivation of the HLLC-type Riemann solver can be found in Appendix B.

3.3 Relaxation procedure

After the evolution step for the fluids approximating (52), (53) the relaxation process solving the system of ordinary differential equations (ODE) (54), (55) has to be performed. Since the relaxation times differ for the different relaxation types, we solve the initial value problem

$$\frac{d\,\boldsymbol{w}(t)}{d\,t} = \boldsymbol{S}^{\xi}(\boldsymbol{w}(t)), \quad t \in [t_n, t_{n+1}], \qquad \boldsymbol{w}(t_n) = \boldsymbol{w}^0 \tag{69}$$

with $\boldsymbol{S}^\xi = ((S^\xi_{\alpha_k})_{k=1,\ldots,K-1}, (S^\xi_{\rho,k}, \boldsymbol{S}^\xi_{\rho\boldsymbol{v},k}, S^\xi_{\rho E,k})_{k=1,\ldots,K})^T$ separately for each relaxation type $\xi \in \{v, p, T, \mu\}$. To avoid the explicit computation of the relaxation times θ_ξ in (31), (32), (33) and (34), we may perform the change of variables $\bar{t} := (t_n - t)\theta_\xi$ and $\overline{\boldsymbol{w}}(\bar{t}) := \boldsymbol{w}(t)$ in (69), i.e.,

$$\frac{d\,\overline{\boldsymbol{w}}(\bar{t})}{d\,\bar{t}} = \frac{1}{\theta^\xi} \boldsymbol{S}^\xi(\overline{\boldsymbol{w}}(\bar{t})), \quad \bar{t} \in [0, \Delta t\theta_\xi], \qquad \overline{\boldsymbol{w}}(0) = \overline{\boldsymbol{w}}^0. \tag{70}$$

Then by definition of the relaxation terms, the relaxation parameter cancels on the right-hand side of (70). Since for all relaxation processes the conservation constraints (8) are satisfied we conclude from (69) that

$$\sum_{k=1}^K \frac{d\,\overline{\alpha}_k(\bar{t})}{d\,\bar{t}} = 0, \ \frac{d\,\overline{\rho}(\bar{t})}{d\,\bar{t}} = 0, \ \frac{d\,(\overline{\rho}\,\overline{\boldsymbol{v}})(\bar{t})}{d\,\bar{t}} = \boldsymbol{0}, \ \frac{d\,(\overline{\rho E})(\bar{t})}{d\,\bar{t}} = 0. \tag{71}$$

Hence, the bulk quantities (9) for density, momentum and energy as well as the saturation condition (1) remain constant during the relaxation process and it holds

$$\sum_{k=1}^K \alpha_k^\infty = \sum_{k=1}^K \alpha_k^0 = 1, \ \rho^\infty = \rho^0, \ (\rho\,\boldsymbol{v})^\infty = (\rho\,\boldsymbol{v})^0, \ (\rho E)^\infty = (\rho E)^0. \tag{72}$$

Furthermore, the conservation of bulk mass and momentum imply that the bulk velocity remains constant

$$\frac{d\,\overline{\boldsymbol{v}}}{d\,\bar{t}} = \boldsymbol{0} \tag{73}$$

and it holds

$$\boldsymbol{v}^\infty = \boldsymbol{v}^0. \tag{74}$$

As already discussed in Section 2.3 we are only interested in the equilibrium state rather the transient relaxation behavior. Therefore we assume that the relaxation process is infinitely fast, i.e., $\theta_\xi \to \infty$ and we do not need to model the relaxation parameters. To compute the equilibrium state, where the source terms (31), (32), (33) and (34) vanish, we perform integration of the ODE system to infinity. This results in a system of algebraic equations for the equilibrium state that will be derived and solved in the subsequent sections. For ease of notation we will use $\boldsymbol{w}$ instead of $\overline{\boldsymbol{w}}$ in (70). In the following we consider one by one the different relaxation processes to equilibrium. Note that the equilibrium state is independent of the order of the relaxation procedures.

3.3.1 Velocity relaxation

In order to determine the equilibrium state of the velocity relaxation process we proceed similar to Saurel and LeMetayer in [39]. The equilibrium state of the velocity relaxation process is determined by solving the system of ODEs

$$\frac{d\,\alpha_k}{d\,\bar{t}} = 0, \tag{75}$$

$$\frac{d\,\alpha_k\,\rho_k}{d\,\bar{t}} = 0, \tag{76}$$

$$\frac{d\,\alpha_k\,\rho_k\,\boldsymbol{v}_k}{d\,\bar{t}} = \alpha_k\,\rho_k(\boldsymbol{v} - \boldsymbol{v}_k), \tag{77}$$

$$\frac{d\,\alpha_k\,\rho_k\,E_k}{d\,\bar{t}} = \alpha_k\,\rho_k\,\boldsymbol{v} \cdot (\boldsymbol{v} - \boldsymbol{v}_k) \tag{78}$$

resulting from (70) with the source terms (32). Since we assume that the relaxation process is infinitely fast, the solution of the system of ODEs converges towards the equilibrium state where the right-hand side vanishes. This holds true for

$$\boldsymbol{v}_k = \boldsymbol{v}^\infty, \quad \bar{t} \to \infty. \tag{79}$$

Integration of (75), (76) over $[0, \infty]$ then results in the algebraic equations

$$\alpha_k^\infty = \alpha_k^0, \tag{80}$$

$$\alpha_k^\infty\,\rho_k^\infty = \alpha_k^0\,\rho_k^0 \quad \text{equiv.} \quad \rho_k^\infty = \rho_k^0. \tag{81}$$

From the equilibrium condition (79) and (74) we conclude that

$$\boldsymbol{v}_k^\infty = \boldsymbol{v}^\infty = \boldsymbol{v}^0. \tag{82}$$

To determine the energy at equilibrium we first observe that by (77) and (78)

$$\frac{d\,\alpha_k\,\rho_k\,E_k}{d\,\bar{t}} = \boldsymbol{v}\,\frac{d\,\alpha_k\,\rho_k\,\boldsymbol{v}_k}{d\,\bar{t}}. \tag{83}$$

Since the bulk velocity remains constant according to (73), we obtain by integration of (83) over $[0,\infty]$ and (82)

$$\alpha_k^\infty\,\rho_k^\infty\,E_k^\infty = \alpha_k^0\,\rho_k^0\,E_k^0 + \alpha_k^0\,\rho_k^0\,\boldsymbol{v}^0\cdot(\boldsymbol{v}^0 - \boldsymbol{v}_k^0) \tag{84}$$

or, equivalently by (81),

$$E_k^\infty = E_k^0 + \boldsymbol{v}^0\cdot(\boldsymbol{v}^0 - \boldsymbol{v}_k^0). \tag{85}$$

Finally, we end up with the algebraic system (74), (80), (81), (82) and (85) by which we determine the velocity equilibrium state. The equilibrium state coincides with the results of Saurel and LeMetayer in [39] for the two-phase model although the derivation is slightly different considering e instead of E.

3.3.2 Pressure relaxation

The equilibrium state of the pressure relaxation process is determined by solving the system of ODEs

$$\frac{d\,\alpha_k}{d\,\bar{t}} = \alpha_k\,(p_k - p), \tag{86}$$

$$\frac{d\,\alpha_k\,\rho_k}{d\,\bar{t}} = 0, \tag{87}$$

$$\frac{d\,\alpha_k\,\rho_k\,\boldsymbol{v}_k}{d\,\bar{t}} = \mathbf{0}, \tag{88}$$

$$\frac{d\,\alpha_k\,\rho_k\,E_k}{d\,\bar{t}} = \alpha_k\,p\,(p - p_k) \tag{89}$$

resulting from (70) with the source terms (31). Again we assume that the relaxation process is infinitely fast, such that the solution of the system of ODEs converges towards the equilibrium state, where the right-hand side vanishes. This holds true for

$$p_k = p^\infty, \quad \bar{t} \to \infty. \tag{90}$$

From (87) and (88) we immediately conclude the conservation of mass and momentum, i.e.,

$$\alpha_k^\infty\rho_k^\infty = \alpha_k^0\rho_k^0, \tag{91}$$

$$\boldsymbol{v}_k^\infty = \boldsymbol{v}_k^0. \tag{92}$$

Furthermore we deduce by (86) and (89) that

$$\frac{d\,\alpha_k\rho_k e_k}{d\,\bar{t}} = \frac{d\,\alpha_k\rho_k E_k}{d\,\bar{t}} = -p\frac{d\,\alpha_k}{d\,\bar{t}}.$$

Integration over $[0,\infty]$ then yields

$$\alpha_k^0\rho_k^0(e_k^\infty - e_k^0) = -\bar{p}(\alpha_k^\infty - \alpha_k^0)$$

with some intermediate interfacial pressure state $\bar{p}$. Following [26] we use the approximation

$$\bar{p} \approx \frac{p^0 + p^\infty}{2} \tag{93}$$

and obtain

$$e_k^\infty = e_k^0 - \frac{p^\infty + p^0}{2\alpha_k^0\rho_k^0}(\alpha_k^\infty - \alpha_k^0). \tag{94}$$

The conservation of mass (91) together with the equations of state (22), equation (94) and the saturation condition (1) give a non-linear algebraic system of $3K + 1$ equations for the $3K + 1$ unknowns α_k^∞, ρ_k^∞, e_k^∞ and p^∞. This system can be reduced. For this purpose we substitute in (22) the single-component density ρ_k^∞ by the mass conservation property (91) and the single-component energy e_k^∞ by (94):

$$
\begin{aligned}
p_k^\infty &= (\gamma_k - 1)\rho_k^\infty(e_k^\infty - q_k) - \gamma_k \pi_k \\
&= (\gamma_k - 1)\frac{\alpha_k^0 \rho_k^0}{\alpha_k^\infty}\left(e_k^0 - \frac{p^\infty + p^0}{2\alpha_k^0 \rho_k^0}(\alpha_k^\infty - \alpha_k^0) - q_k\right) - \gamma_k \pi_k.
\end{aligned}
$$

Furthermore we conclude from the equation of state (22) that

$$
e_k^0 = \frac{p_k^0 + \gamma_k \pi_k}{\rho_k^0(\gamma_k - 1)} + q_k
$$

and thus the single-component pressure becomes

$$
p_k^\infty = \frac{\alpha_k^0}{\alpha_k^\infty}(p_k^0 + \gamma_k \pi_k) - \frac{(\gamma_k - 1)(\alpha_k^\infty - \alpha_k^0)}{2\alpha_k^\infty}(p^\infty + p^0) - \gamma_k \pi_k. \tag{95}
$$

Since $p_k^\infty = p^\infty$ holds in the equilibrium state, we finally deduce from the above equation that

$$
p_k^\infty = \frac{a_k \alpha_k^\infty + b_k}{c_k \alpha_k^\infty + d_k}
$$

with

$$
\begin{array}{ll}
a_k = -\left[(\gamma_k - 1)p^0 + 2\gamma_k \pi_k\right], & b_k = (\gamma_k - 1)\alpha_k^0 p^0 + 2\alpha_k^0 p_k^0 + 2\alpha_k^0 \gamma_k \pi_k, \\
c_k = (\gamma_k + 1), & d_k = (1 - \gamma_k)\alpha_k^0.
\end{array}
$$

From the relation $p_1^\infty = p_k^\infty$ we derive

$$
\alpha_k^\infty = \frac{A_k \alpha_1^\infty + B_k}{C_k \alpha_1^\infty + D_k} \tag{96}
$$

with

$$
\begin{array}{ll}
A_k = b_k c_1 - a_1 d_k, & B_k = b_k d_1 - b_1 d_k, \\
C_k = a_1 c_k - a_k c_1, & D_k = b_1 c_k - a_k d_1,
\end{array}
$$

Replacing these relations for α_k^∞, $k = 2\ldots, K$, in the saturation equation (1) we end up with a polynomial of degree K for α_1^∞. Since we are only performing three-component simulations, we give here for convenience of the reader only the third order polynomial for α_1^∞

$$
a(\alpha_1^\infty)^3 + b(\alpha_1^\infty)^2 + b\alpha_1^\infty + d = 0. \tag{97}
$$

The coefficients a, b, c, d are given by the following relations

$$
\begin{aligned}
a &= C_1 C_2, \\
b &= C_1 D_2 + C_2 D_1 + A_1 C_2 + A_2 C_1 - C_1 C_2, \\
c &= D_1 D_2 + A_1 D_2 + B_1 C_2 + A_2 D_1 + B_2 C_1 - C_1 D_2 - C_2 D_1, \\
d &= B_1 D_2 + B_2 D_1 - D_1 D_2.
\end{aligned}
$$

Usually this equation exhibits three solutions. By the conditions $\alpha_k^\infty \in (0, 1)$ and $p^\infty > 0$ we can single out the suitable solution. If there does not exist a unique solution for a given initial state, we stop the computation. This may happen for large pressure difference $p^\infty - p^0$ when the approximation error using (93) becomes significant. Then one may reduce the CFL number or, as suggested in [26], the system of ODEs (86) – (89) is solved approximately by quadrature.

Once, we have computed α_1^∞ we can determine the remaining volume fractions α_k^∞ by (96), the pressures p_k^∞ by (95), the internal energies e_k^∞ by (94). These are completed by the relations (91) and (92) to compute the equilibrium state.

Finally we want to remark that the above procedure to determine the pressure equilibrium state is similar to [26] for a two-phase model and [46] for a two-phase model with three components.

3.3.3 Temperature relaxation

For the temperature relaxation process we have to solve the system of ODEs

$$\frac{d\,\alpha_k}{d\,\bar{t}} = \frac{\alpha_k}{\kappa_k}(\hat{T} - T_k), \tag{98}$$

$$\frac{d\,\alpha_k\,\rho_k}{d\,\bar{t}} = 0, \tag{99}$$

$$\frac{d\,\alpha_k\,\rho_k\,\boldsymbol{v}_k}{d\,\bar{t}} = 0, \tag{100}$$

$$\frac{d\,\alpha_k\,\rho_k\,E_k}{d\,\bar{t}} = \alpha_k\,(\hat{T} - T_k), \tag{101}$$

resulting from (70) with the source terms (33). Since we assume that the relaxation process is infinitely fast, the solution of the system of ODEs converges towards the equilibrium state where the right-hand side vanishes. This holds true for

$$p_k^\infty = p^\infty, \quad T_k^\infty = T^\infty, \qquad \bar{t} \to \infty. \tag{102}$$

Note that we also have to impose pressure equilibrium. Otherwise, the pressures p_k^∞ might not be in equilibrium even if the initial pressures are in equilibrium, i.e., $p_k^0 = p^0$.

From (99) and (100) we again conclude on the conservation of mass and momentum, i.e.,

$$\alpha_k^\infty \rho_k^\infty = \alpha_k^0 \rho_k^0, \tag{103}$$

$$\boldsymbol{v}_k^\infty = \boldsymbol{v}_k^0. \tag{104}$$

Then (101) implies the conservation of the bulk energy

$$\sum_{k=1}^{K}(\alpha_k\rho_k e_k)^\infty = \sum_{k=1}^{K}(\alpha_k\rho_k e_k)^0. \tag{105}$$

Due to the mass conservation (103) and the equation of state (24) this is equivalent to

$$\sum_{k=1}^{K}\alpha_k^\infty \frac{p_k^\infty + \gamma_k\pi_k}{(\gamma_k - 1)} = \sum_{k=1}^{K}\alpha_k^0 \frac{p_k^0 + \gamma_k\pi_k}{(\gamma_k - 1)} =: \Lambda. \tag{106}$$

The temperature equilibrium (102) implies $T_k^\infty = T_{k_0}^\infty$ for all phases k, where we fix an arbitrary phase k_0 to be specified below. Since we also assume pressure equilibrium, i.e., $p_k^\infty = p^\infty$, we conclude together with the equation of state (25) that

$$\alpha_k^\infty = \alpha_{k_0}^\infty \frac{a_k}{a_{k_0}} \frac{p^\infty + \pi_{k_0}}{p^\infty + \pi_k} \quad \text{with} \quad a_k := c_{v,k}(\gamma_k - 1)\alpha_k^0\rho_k^0. \tag{107}$$

Then the saturation condition (1) yields

$$\alpha_{k_0}^\infty = \left(\sum_{k=1}^{K} \frac{a_k}{a_{k_0}} \frac{p^\infty + \pi_{k_0}}{p^\infty + \pi_k}\right)^{-1} \tag{108}$$

We now substitute α_k^∞ in (106) by (107) and then replace $\alpha_{k_0}^\infty$ by (108). For ease of representation we introduce the sets $\mathcal{E} := \{k : \pi_k = \pi_{k_0}, \ k \in \{1, \ldots, K\}\}$ and $\mathcal{N} := \{k : \pi_k \neq \pi_{k_0}, \ k \in \{1, \ldots, K\}\}$. Together with the assumption of pressure equilibrium (102) we finally obtain after some algebraic manipulations

$$\sum_{k\in\mathcal{E}} \frac{a_k}{a_{k_0}} \left(\frac{p^\infty + \gamma_k\pi_k}{\gamma_k - 1} - \Lambda\right) \prod_{l\in\mathcal{N}} (p^\infty + \pi_l) + \tag{109}$$

$$\sum_{k\in\mathcal{N}} \frac{a_k}{a_{k_0}} \left(\frac{p^\infty + \gamma_k\pi_k}{\gamma_k - 1} - \Lambda\right) (p^\infty + \pi_{k_0}) \prod_{l\in\mathcal{N}, l\neq k} (p^\infty + \pi_l) = 0.$$

Hence, the equilibrium pressure p^∞ is characterized as the root of a polynomial of degree $\#\mathcal{N} + 1$. By the conditions $\alpha_k^\infty \in (0, 1)$ and $p^\infty > 0$ we may single out the unique physically admissible solution as we will do for some models at the end of this section. To reduce the number of roots we therefore recommend that the index k_0 should be chosen such that the cardinality of $\mathcal{N}$ is smallest. In particular, if all π_k coincide, then we may compute p^∞ directly as

$$p^\infty = \sum_{k=1}^K \frac{a_k}{a_{k_0}} \left(\Lambda - \frac{\gamma_k \pi_k}{\gamma_k - 1} \right) \left(\sum_{k=1}^K \frac{a_k}{a_{k_0}} \frac{1}{\gamma_k - 1} \right)^{-1}.$$

Another special case is the three-component model composed of water vapor, liquid water and gas, see Section 2.3 and Table 1. Choosing $k_0 = 1$ and multiplying (109) by $a_{k_0} = a_1$ we then obtain the quadratic polynomial

$$A\,(p^\infty)^2 + B\,p^\infty + C = 0, \tag{110}$$

where the coefficients are determined by

$$
\begin{aligned}
A &:= \sum_{k=1}^3 \frac{a_k}{\gamma_k - 1}, \\
B &:= a_1 \left(\frac{\gamma_1 \pi_1 + \pi_2}{\gamma_1 - 1} - \Lambda \right) + a_2 \left(\frac{\gamma_2 \pi_2 + \pi_1}{\gamma_2 - 1} - \Lambda \right) + a_3 \left(\frac{\gamma_3 \pi_3 + \pi_2}{\gamma_3 - 1} - \Lambda \right), \\
C &:= a_1 \pi_2 \left(\frac{\gamma_1 \pi_1}{\gamma_1 - 1} - \Lambda \right) + a_2 \pi_1 \left(\frac{\gamma_2 \pi_2}{\gamma_2 - 1} - \Lambda \right) + a_3 \pi_2 \left(\frac{\gamma_3 \pi_3}{\gamma_3 - 1} - \Lambda \right).
\end{aligned}
$$

Note that the equilibrium temperature T^∞ may be directly computed from the equilibrium pressure. Starting from the equation of state (25) we first employ mass conservation (103) and replace α_k^∞ by (107) and (108). Finally we obtain together with (108)

$$T_k^\infty = \left(\sum_{l=1}^K \frac{a_l}{p^\infty + \pi_l} \right)^{-1} = T^\infty \tag{111}$$

After having determined p^∞, the volume fractions $\alpha_{k_0}^\infty$ and α_k^∞, $k \neq k_0$, can be computed by (108) and (107), respectively. Then the mass conservation (103) provides us with ρ_k^∞. Finally we compute the internal energies e_k^∞ according to the equation of state (24).

We conclude this section with some remarks on the physically admissible solution of (109) confining ourselves to the following three models:

Two-component gas model: In this case $\pi_1 = \pi_2 = 0$ and there only exists one root of (109)

$$p^\infty = \frac{(a_1 + a_2)\,\Lambda}{a_1/(\gamma_1 - 1) + a_2/(\gamma_2 - 1)} > 0.$$

According to (108) and (107) as well as (111) we compute the corresponding equilibrium states for the volume fractions and the temperature, respectively, as

$$\alpha_k^\infty = \frac{a_k}{a_1 + a_2} \in [0, 1], \; k = 1, 2, \qquad T^\infty = \frac{p^\infty}{a_1 + a_2} > 0.$$

Two-phase model: In this case $\pi_2 \neq \pi_1 = 0$. There exist two roots of (110) with $a_3 = 0$ because $A = a_1/(\gamma_1 - 1) + a_2/(\gamma_2 - 1) > 0$ and $C = -a_1 \Lambda \pi_2 < 0$. The only admissible solution is

$$p^\infty = -\frac{B}{2A} + \sqrt{\frac{B^2}{4A^2} - \frac{C}{A}} > 0. \tag{112}$$

From (108) and (111) we then conclude

$$\alpha_1^\infty = \frac{a_1(p^\infty + \pi_2)}{(a_1 + a_2)p^\infty + a_1 \pi_2} = 1 - \alpha_1^\infty \in [0, 1], \quad T^\infty = \frac{p^\infty(p^\infty + \pi_2)}{(a_1 + a_2)p^\infty + a_1 \pi_2} > 0.$$

Three-component model: In this case we assume that $\pi_1 = \pi_2 \neq \pi_3$. Then we observe that again $A > 0$ and $C < 0$ in (110) and thus (112) is the only admissible root. From (108), (107) and (111) we then conclude $\alpha_1 \in [0, 1]$, $\alpha_2, \alpha_2 > 0$ and $T^\infty > 0$.

3.3.4 Relaxation of chemical potentials

The equilibrium state of the chemical potential relaxation process is determined by solving the system of ODEs

$$\frac{d\,\alpha_k}{d\,\bar{t}} = \frac{\dot{m}}{\varrho_k}, \ \ k = 1, 2, \quad \frac{d\,\alpha_3}{d\,\bar{t}} = -\dot{m}\left(\frac{1}{\varrho_1} + \frac{1}{\varrho_2}\right), \tag{113}$$

$$\frac{d\,\alpha_k\,\rho_k}{d\,\bar{t}} = (-1)^{k+1}\dot{m}, \ \ k = 1, 2, \quad \frac{d\,\alpha_3\,\rho_3}{d\,\bar{t}} = 0, \tag{114}$$

$$\frac{d\,\alpha_k\,\rho_k\,\boldsymbol{v}_k}{d\,\bar{t}} = (-1)^{k+1}\dot{m}\,\boldsymbol{V}_I, \ \ k = 1, 2, \quad \frac{d\,\alpha_3\,\rho_3\,\boldsymbol{v}_3}{d\,\bar{t}} = \boldsymbol{0}, \tag{115}$$

$$\frac{d\,\alpha_k\,\rho_k\,E_k}{d\,\bar{t}} = (-1)^{k+1}\dot{m}\left(\epsilon_k + \frac{\boldsymbol{V}_I^2}{2}\right), \ \ k = 1, 2, \quad \frac{d\,\alpha_3\,\rho_3\,E_3}{d\,\bar{t}} = \dot{m}\,(\epsilon_2 - \epsilon_1) \tag{116}$$

resulting from (70) with the source terms (34). Again we assume that the relaxation process is infinitely fast such that the solution of the system of ODEs converges towards the equilibrium state, where the right-hand side vanishes. According to [46, 48] this holds true for

$$p_1^\infty = p_2^\infty = p_3^\infty \ = \ p^\infty, \quad \bar{t} \to \infty, \tag{117}$$
$$T_1^1 = T_2^1 = T_3^1 \ = \ T^\infty, \quad \bar{t} \to \infty, \tag{118}$$
$$\mu_1^\infty \ = \ g_2^\infty, \quad \bar{t} \to \infty. \tag{119}$$

Note that due to these equilibrium conditions the muss flux $\dot{m}$ vanishes at equilibrium and, thus, the right-hand sides in (113), (114), (115) and (116) become zero. Obviously, the equations (113) are in agreement with the saturation condition (1), i.e.,

$$\alpha_1^\infty + \alpha_2^\infty + \alpha_3^\infty = 1. \tag{120}$$

The mass equations (114) induce

$$\alpha_3^\infty\,\rho_3^\infty \ = \ \alpha_3^0\rho_3^0, \tag{121}$$
$$\alpha_1^\infty\,\rho_1^\infty + \alpha_2^\infty\,\rho_2^\infty \ = \ \alpha_1^0\rho_1^0 + \alpha_2^0\rho_2^0 =: W\,. \tag{122}$$

Furthermore, we assume that the single-component velocities are initially in equilibrium and stay in equilibrium during the relaxation of the chemical potentials, i.e.,

$$\boldsymbol{v}^\infty = \boldsymbol{v}_k^\infty = \boldsymbol{v}_k^0 = \boldsymbol{v}^0, \quad k = 1, 2, 3. \tag{123}$$

Note that this holds true for component $k = 3$ according to (114) and (115). Then we conclude with (116) that

$$\sum_{k=1}^{3} \alpha_k^\infty\,\rho_k^\infty\,e_k^\infty = \sum_{k=1}^{3} \alpha_k^0\rho_k^0 e_k^0 =: E\,. \tag{124}$$

Motivated by the equilibrium condition (119) the aim is now to derive a function

$$f_\mu(\alpha_1\rho_1) := \mu_1^\infty(\alpha_1\rho_1) - g_2^\infty(\alpha_1\rho_1) \tag{125}$$

depending only on the product $\alpha_1\rho_1$ such that the root $\alpha_1^\infty\rho_1^\infty$ is the solution for the relaxed mass density for the first component. For this purpose we have to express α_1^∞, α_2^∞, T^∞ and p^∞ in terms of $\alpha_1^\infty\rho_1^\infty$. Then the chemical potential for water vapor μ_2 and the Gibbs free energies g_k, $k = 1, 2$, see Section 2.2, can be written as

$$\mu_1^\infty(\alpha_1\rho_1) \ = \ g_1^\infty(\alpha_1\rho_1) + \frac{\kappa_b}{m_{01}}T^\infty(\alpha_1\rho_1)\ln\left(\frac{\alpha_1(\alpha_1\rho_1)}{1 - \alpha_2(\alpha_1\rho_1)}\right) \tag{126}$$

$$g_k^\infty(\alpha_1\rho_1) \ = \ (c_{v,k}\gamma_k - q_k')T^\infty(\alpha_1\rho_1) - c_{v,k}\gamma_k T^\infty(\alpha_1\rho_1)\ln(T^\infty(\alpha_1\rho_1)) +$$
$$T^\infty(\alpha_1\rho_1)c_{v,k}(\gamma_k - 1)\ln(p^\infty(\alpha_1\rho_1) + \pi_k) + q_k, \tag{127}$$

where

$$\kappa_b = 1.380656 \cdot 10^{-23}\,\frac{J}{K} \quad \text{and} \quad m_{01} = \frac{2 \cdot 1.0079 + 15.9994}{6.02205 \cdot 10^{26}}kg$$

denote the Boltzmann constant and the mass of a single water molecule, respectively.

Note that a root of (125) may not exist. Beside the existence of an equilibrium solution the water vapor may completely condensate or the liquid water may completely evaporate. Therefore in a first step one has to figure out, which of the four cases occurs:

(i-a) condensation process with equilibrium solution,

(i-b) total condensation,

(ii-a) evaporation process with equilibrium solution,

(ii-b) total evaporation.

In case (i-b) and (ii-b) the result can be directly obtained. In the cases (i-a) and (ii-a) a bisection method is provided to find the equilibrium state. Due to the fact that the temperature relaxation method is simple and always gives a unique, physical solution, we base the bisection method to find the equilibrium state on the temperature relaxation procedure.

According to thermodynamics a condensation process and an evaporation process are characterized by a positive or negative sign of $\mu_1 - g_2$, respectively. Thus, using the data from the temperature relaxation procedure we may identify condensation and evaporation processes.

Condensation. If a condensation process is identified by $\mu_1 - g_2 > 0$ the expression $\alpha_1^0 \rho_1^0$ is too large and $\alpha_1 \rho_1$ has to decrease. The smallest admissible value for this expression is $\alpha_1^* \rho_1^* = tol > 0$. This means that all water vapor has condensated except a small amount due to numerical reasons. Using the temperature relaxation procedure according to Section 3.3.3 with $\alpha_1^* \rho_1^*$ instead of $\alpha_1^0 \rho_1^0$ we determine the corresponding values for all variables of the phases. Using these data one has to check the sign of the difference of the chemical potentials. If still $\mu_1 - g_2 > 0$ holds, then total condensation will occur. We keep $\alpha_1^* \rho_1^* = tol > 0$ and the corresponding data. Otherwise the interval $[\alpha_1^* \rho_1^* = tol, \alpha_1^0 \rho_1^0]$ is admissible for the bisection method.

Evaporation. If an evaporation process is identified by $\mu_1 - g_2 < 0$ the expression $\alpha_1^0 \rho_1^0$ is too small and $\alpha_1 \rho_1$ has to increase. Because of (122) we have the bound $\alpha_1^* \rho_1^* \leq W$. Moreover, we have to guarantee that

$$E - \alpha_1 \rho_1 q_1 - W q_2 + \alpha_1 \rho_1 q_2 = \sum_{k=1}^{3} \alpha_k \frac{p + \gamma_k \pi_k}{\gamma_k - 1} \geq 0 \, .$$

Here the left-hand side is derived from (124) where we plug in (122) and (24) and use $\pi_1 = 0$ and $q_3 = 0$. Thus we conclude

$$\alpha_1^* \rho_1^* = \min \left\{ W - tol, \frac{E - W q_2}{q_1 - q_2} \right\} \, .$$

Again using the temperature relaxation procedure according to Section 3.3.3 with $\alpha_1^* \rho_1^*$ instead of $\alpha_1^0 \rho_1^0$ we find the corresponding values for all variables of the phases. Using these data one has to check the sign of the difference of the chemical potentials. If still $\mu_1 - g_2 < 0$ holds, then total evaporation will occur. We keep $\alpha_1^* \rho_1^* = tol > 0$ and the corresponding data. Otherwise the interval $[\alpha_1^0 \rho_1^0, \alpha_1^* \rho_1^*]$ is admissible for the bisection method.

Finally we summarize the relaxation of chemical potential.

Algorithm.

1. Identify condensation or evaporation processes (i) or (ii).

2. Check, whether an equilibrium solution exists; this leads to four possible cases (i-a), (i-b), (ii-a), (ii-b):

   - if (i-a): apply the bisection method to find the root of (125) in the interval $[\alpha_1^* \rho_1^* = tol, \alpha_1^0 \rho_1^0]$

   - if (i-b): apply the temperature relaxation procedure with $\alpha_1^* \rho_1^* = tol$

   - if (ii-a): apply the bisection method to find the root of (125) in the interval $[\alpha_1^0 \rho_1^0, \alpha_1^* \rho_1^*]$ with $\alpha_1^* \rho_1^* = \min \left\{ W - tol, \frac{E - W q_2}{q_1 - q_2} \right\}$

- if (ii-b): apply the temperature relaxation procedure with $\alpha_1^* \rho_1^* = W - tol$

The above relaxation procedure can be considered an essential improvement of the original one presented in [46, 48] due to the following aspects: In the original procedure the Gibbs free energies are relaxed, i.e., the influence of the mixture entropy, which is described by the difference of the chemical potential and the Gibbs free energy of the vapor phase, is neglected. This extra term cancels in pure phases. Moreover, in the original procedure a double iteration method was used. We now reduce the numerical costs significantly by simplifying the equilibrium system to a *scalar* equation depending only on $\alpha_1 \rho_1$ that has to be solved by a *single* iteration process.

3.3.5   Application of relaxation procedures

We conclude the section on the relaxation to equilibrium by some remarks on (i) the order of performing the relaxation procedures and (ii) where to apply them.
From a physical point of view the equilibrium state should not depend on the order of the relaxation processes. For instance, performing relaxation of the chemical potentials does not require to perform mechanical and thermal relaxation before. According to (117) and (118) pressures and temperatures are relaxed to equilibrium together with the mass. On the other hand, the equilibrium velocity is not changed by neither of the other relaxation procedures and vice versa as becomes obvious from the definition (31), (32), (33) and (34) of the relaxation terms. However, from a numerical point of view performing the latter relaxation procedures will provide a better initial guess for the bisection method involved in performing the mass transfer.
For the same reasons we do not have to perform pressure relaxation first when performing temperature relaxation without accounting for mass transfer, see Section 3.3.3, because the pressures are relaxed simultaneously to equilibrium together with the temperatures according to (102).

Since by both the thermal and the chemical relaxation procedure we also relax the pressures simultaneously there is no need to perform the pressure relaxation, see Section 3.3.2. The advantage is twofold: First of all, for our three-component model we do not have to compute the roots of the cubic polynomial (97) but the quadratic polynomial (110) where the admissible root can be singled out apriorily. Furthermore, we avoid the approximation step (93) as usually performed, cf. [47, 48, 34], that can cause instabilities in case of strong non-equilibrium, i.e., the differences $p_k^0 - p^\infty$ are large. In particular, we observe that by the pressure relaxation small oscillations may be triggered that spoil significantly the performance of locally adaptive computations due to denser grids. Consequently, the computational costs of our computations could be significantly reduced.

Furthermore we strongly recommend that temperature relaxation should always be accounted for in the computations. For the investigation of a bubble collapse, see Section 4.2, it turned out that without temperature relaxation there will be unphysically high temperatures for water vapor and inert gas that can take values in the order of 100000 K. This will cause high sound speeds that trigger very small time discretizations due to the CFL number. When performing the same computation with temperature relaxation, the equilibrium temperatures stay in a physically admissible range and the computations will be much faster because the CFL number is moderate and the time discretization does not become as small as before.

Finally, we note that after each evolution step the phases may be in non-equilibrium. Therefore the relaxation procedures have to be performed in *each* cell of the computational domain. In [46] an interfacial region or a mixture zone has been introduced to avoid *unphysical* nucleation or cavitation. In Section 4.1 we will verify that these do not occur in our model due to the sign of the difference of the chemical potentials. On the other hand, the model is able to describe *physical* cavitation by expansion. For this reason we avoid introducing an artificial interfacial region to avoid numerical instabilities.

4   Numerical results

To verify our model we investigate three different configurations, namely, (i) one-dimensional Riemann problems, (ii) quasi-one-dimensional bubble collapse and (iii)quasi-two-dimensional shock-bubble interaction. For all these configurations we apply the three-component model with water vapor, liquid water and inert gas with the material parameters listed in Table 1. The relaxation process is modeled by the procedures for the velocity relaxation, the temperature relaxation and the relaxation of chemical potentials according to Sections 3.3.1, 3.3.3 and 3.3.4, respectively. These are applied after the time evolution of the conserved quantities in this order. Note that by the procedure of the temperature relaxation the pressures will also be in equilibrium.

The efficiency of the scheme is improved by local grid adaption where we employ the multiresolution concept based on biorthogonal wavelets. The key idea is to perform a multiresolution analysis on a sequence of nested grids providing a decomposition of the data on a coarse scale and a sequence of details that encode the difference of approximations on subsequent resolution levels. The detail coefficients become small when the underlying data are locally smooth and, hence, can be discarded when dropping below a threshold value ε_{thresh}. By means of the thresholded sequence a new, locally refined grid is determined. Details on this concept can be found in [31, 32].

4.1   Real cavitation

Cavitation induced by expansion is a frequently investigated problem in the literature. For instance, in [47] an expansion tube filled with liquid water is investigated. For numerical reasons it is necessary that some amount of vapor exists initially. In [47] a large initial vapor volume fraction, $\alpha_{vapor} = 0.01$, was necessary due to the definition of an interfacial region and the constraints for the thermal relaxation procedures. Here we use $\alpha_{vapor} = 10^{-8}$. Although the vapor volume fraction may decrease during the computation it always stays positive. This also holds true for all phases that may be initialized by a small value. Furthermore, we avoid to introduce technical parameters, e.g., the definition of an interfacial region or a tolerance range $[\bar{\epsilon}, 1 - \bar{\epsilon}]$ for the volume fractions. These may trigger oscillations and unphysical phenomena in the solution, e.g. wave splitting. Nevertheless, we are able to simulate cavitation *without* causing unphysical cavitation. For illustration we consider two symmetric examples where the pressure, velocity and temperature of each component is in equilibrium. The volume fractions as well as the pressure and the velocity are constant, whereas the velocity exhibits a discontinuity. The fluid consists of almost pure liquid water perturbed by a small amount $\varepsilon = 10^{-8}$ of the other components. The parameters are listed in Table 2.

	α_{vapor}	α_{water}	p [bar]	T [K]	v_{left} [m/s]	v_{right} [m/s]
C1	ε	$1 - 2\varepsilon$	1	293	-10	+10
C2	ε	$1 - 2\varepsilon$	1	293	+10	-10

Table 2: Initial data for Riemann problems: Expansion (C1) and compression (C2) of water with $\varepsilon = 10^{-8}$.

For all our computations, the computational domain is $\Omega = [0, 1]$ m, where for boundary conditions we set the initial left and right state, respectively. The initial jump is located at $x = 0.5$ m. The domain is discretized by $N_0 = 5$ cells on coarsest level and successively refined using $L = 10$ refinement levels. The threshold value is set to $\varepsilon_{thresh} = 10^{-4}$. The temporal discretization is adjusted during the computation by a fixed CFL number of 0.5. The computations terminate at the final time $T = 2 \times 10^{-4}$ s.

In Example C1 the almost pure liquid water phase is expanded and the pressure drops. This leads to cavitation, i.e., water vapor is created due to the phase transition where mass is transferred from liquid water to water vapor, see Figure 1. Thus we can simulate cavitation *without* having initialized a significant amount of water vapor.

Next we present the results for Example C2, see Figure 2. The liquid phase is now compressed. The water volume fraction remains constant, i.e., no unphysical cavitation occurs. This

confirms that we do not have to introduce an interfacial region but may perform relaxation of chemical potentials throughout the computational domain.
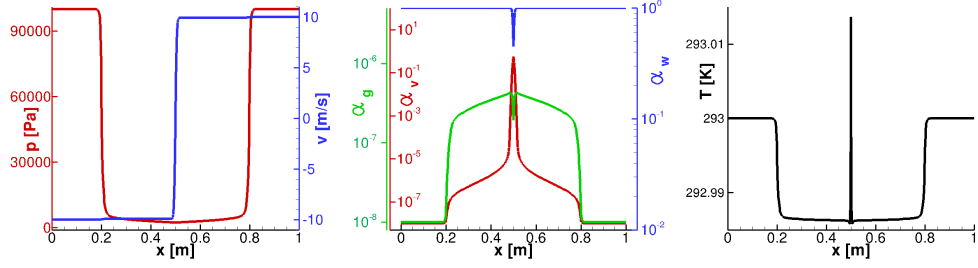

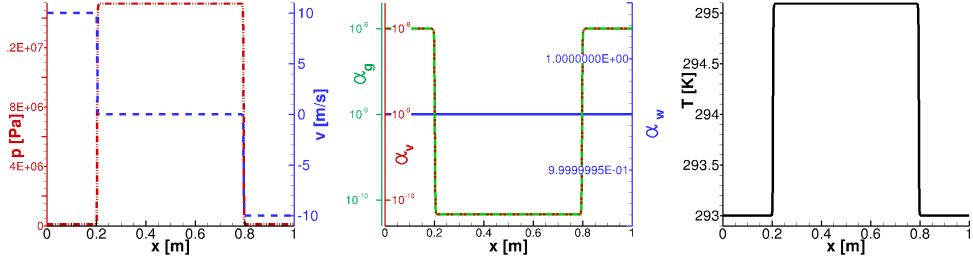Figure 1: Example C1: Pressure and velocity (left), volume fractions (middle) and temperature (right).

Figure 2: Example C2: Pressure and velocity (left), volume fractions (middle) and temperature (right).

4.2   Spherical bubble collapse

The collapse of a vapor-filled spherical bubble in water is a classical problem that has been extensively investigated in the literature. There are simplified models available such as Rayleigh-Plesset [35], Gilmore [18], Keller-Mikis [25], etc. that provide a good approximation of the bubble radius. However, the prediction of the rebound and further oscillations are not well predicted. The first collapse is dominated by incompressibility effects, whereas in the collapse other effects such as compressibility and phase transition become effective. These are not properly taken into account in the aforementioned models. Furthermore, these simplified models provide no insight to the attached flow field neither in the liquid nor in the bubble.

In experiments performed with laser-induced cavitation bubbles, cf. [14, 41, 44] it was verified that the water temperature significantly affects the rebound. By heating the water the vapor pressure is increased which leads to a high vapor content, i.e., low amount of non-condensable gas, and the bubble collapses more mildly due to a stronger damping. In particular, the increase in the vapor pressure results in a larger maximum bubble radius, and, thus, the collapse time is extended and the rebound is more pronounced.

Motivated by these experiments we want to investigate the influence of non-condensable gas on the bubble collapse and its rebound by performing numerical simulations with the three-component model for water vapor, liquid water and inert gas, see Section 2. Of special interest are the bubble radius, temperature and gas volume fraction inside the bubble as well as grid convergence for both with and without mass transfer. The corresponding material parameters for the stiffened gas equation of state are listed in Table 1. Since the experiments cannot provide the state inside the bubble, we perform a parameter study for a bubble with maximal radius $R_{max} = 0.75$ mm where we vary the amount of non-condensable gas instead of the water temperature in the experiments. In particular, the water state is always chosen as $p = 100000$

bubble	p [Pa]	T [K]	α_{vapor} [-]	α_{water} [-]	α_{gas} [-]
G05	2339	293	0.949999	10^{-8}	0.05
G10	2339	293	0.899999	10^{-8}	0.10
G20	2339	293	0.799999	10^{-8}	0.20
G40	2339	293	0.599999	10^{-8}	0.4
liquid	100000	293	10^{-6}	0.999998	10^{-6}

Table 3: Initial Data inside the bubble and in the liquid.

bubble	x_{vapor} [-]	x_{water} [-]	x_{gas} [-]	x_{vapor}/x_{gas} [-]
G05	0.9944	0.00051	0.00508	195.6
G10	0.9888	0.00054	0.01067	92.7
G20	0.9757	0.00060	0.02369	41.2
G40	0.9385	0.00077	0.06077	15.4

Table 4: Mass fractions corresponding to initial data inside the bubble.

Pa, $T = 293$ K. Inside the bubble we always set the vapor pressure $p = 2339$ Pa at $T = 293$ K but vary the volume fraction of gas from 0.05, 0.1, 0.2 to 0.4 corresponding to case G05, G10, G20 and G40, respectively. Note that the model does not allow for vanishing phases, because we need to divide by the volume fraction in order to compute the pressure of a pure phase. Therefore we have to add a small amount of vapor and non-condensable gas in the liquid environment, i.e., $\alpha_{gas} = \alpha_{vapor} = 10^{-6}$, and vice versa some tiny amount of water inside the bubble, i.e., $\alpha_{water} = 10^{-8}$. Since the water density is much larger than the densities of the gas and the vapor, the artificial amount of water is chosen much smaller. The initial data for the computations are summarized in Table 3. All components inside and outside the bubble are assumed to be in equilibrium. The corresponding densities are computed from the equations of state (22) and (23). In Table 4 we also list the mass fraction of the phases inside the bubble. We note that the artificial state of liquid water does not significantly pollute the gaseous states inside the bubble.

Since the problem is inherently one-dimensional due to spherical symmetry, we perform quasi-one-dimensional computations where we have to take the change of metric into account in the fluid discretization (56) and (57). The resulting scheme in radial direction r thus reads

$$(\alpha_k)_i^{n+1} = (\alpha_k)_i^n - \frac{\Delta t}{\Delta r^3} \left(r_{i+\frac{1}{2}}(\overline{V_I})_{i,i+1}(\alpha_k')_{i,i+1}^n - r_{i-\frac{1}{2}}(\overline{V_I})_{i-1,i}(\alpha_k')_{i-1,i}^n \right), \qquad (128)$$

$$(\boldsymbol{u}_k)_i^{n+1} = (\boldsymbol{u}_k)_i^n - \frac{\Delta t}{\Delta r^3} \left(r_{i+\frac{1}{2}}\boldsymbol{G}_{i,i+1}^n - r_{i-\frac{1}{2}}\boldsymbol{G}_{i-1,i}^n \right) + 2\,\hat{r}_i \frac{\Delta r \Delta t}{\Delta r^3} \boldsymbol{S}_k(\boldsymbol{w}_i^n), \qquad (129)$$

where the fluxes and the derivatives of the volume fractions are determined by

$$\begin{aligned}
\boldsymbol{G}_{i,i+1}^n &:= \boldsymbol{F}_k(\boldsymbol{w}_{i,i+1}^n, \boldsymbol{w}_{i+1,i}^n) - \boldsymbol{H}(\overline{\boldsymbol{w}}_{i,i+1})(\alpha_k')_{i,i+1}^n, \\
\boldsymbol{G}_{i-1,i}^n &:= \boldsymbol{F}_k(\boldsymbol{w}_{i-1,i}^n, \boldsymbol{w}_{i-1,i}^n) - \boldsymbol{H}(\overline{\boldsymbol{w}}_{i-1,i})(\alpha_k')_{i-1,i}^n, \\
(\alpha_k')_{i,i+1}^n &:= ((\overline{\alpha}_k)_{i,i+1} - (\alpha_k)_i^n), \quad (\alpha_k')_{i-1,i}^n := ((\overline{\alpha}_k)_{i-1,i} - (\alpha_k)_i^n).
\end{aligned}$$

Since in each time step pressure is at equilibrium, we employ here the identity (51). Note that $\boldsymbol{u}_k = \alpha_k(\rho_k, \rho_k v_k, E_k)^T$ is now composed of the density, the momentum in radial direction and total energy of component k and $\boldsymbol{H}(\boldsymbol{w}) = (0, P_I, P_I V_I)^T$ is now a vector. The additional metric term is defined by $\boldsymbol{S}_k(\boldsymbol{w}) = (0, \alpha_k p_k, 0)^T$. The metric is determined by $\hat{r}_i = 0.5(r_{i+\frac{1}{2}} + r_{i-\frac{1}{2}})$ and $\Delta r^3 = (r_{i+\frac{1}{2}}^3 + r_{i-\frac{1}{2}}^3)/3$. This quasi-one-dimensional scheme can be derived from the three-dimensional discretization applied to a special grid similar to [33]. A detailed derivation is given in Appendix C.

For all our computations, the computational domain is $\Omega = [0, 0.384]$ m, where for boundary conditions we choose symmetry and reflecting boundary conditions at the left and the right boundary, respectively. The bubble center is located at $r = R_{max}$. The domain is largely extended to the right to avoid interaction of waves emanating from the right boundary with

the collapsing bubble in the investigated time interval. The domain is discretized by $N_0 = 16$ cells on coarsest level and successively refined using $L = 16$ refinement levels, i.e., there are $N_{16} = 1048576$ cells on a uniformly refined grid with $N_{I,L} = 2048$ cells located within the initial bubble with radius $r_I = R_{max}$. The threshold value is always set to $\varepsilon_{thresh} = 10^{-3}$. For the time discretization we choose a constant CFL number 0.8. The computations terminated at $T = 240$ μs.

Bubble Radius. First of all, we investigate the influence of the amount of non-condensable gas on the bubble radius. In Figure 3, we show for all cases the transient bubble radius identified by the water volume fraction $\alpha_{water} = 0.5$. For comparison we also plot the radii that have been deduced from an experiment with laser-induced cavitation bubbles and are taken from [33]. We observe that in the first collapse the bubble radius and the collapse time is not affected by the varying gas fraction and agrees perfectly with the experiment. This holds true for both computations with and without mass transfer. Obviously, phase transition is not effective at this stage whereas mechanical processes are dominating. However, at the instant of the collapse the minimal bubble radius becomes larger, i.e., the collapse is milder, and the rebound is the stronger the higher the amount of non-condensable gas. Thus the time for the subsequent collapses increases as well. This phenomena can be explained by a spring that is loaded in the collapse and releases when the bubble expands again. The tension of the spring is higher with increasing amount of gas inside the bubble. However, when neglecting the mass transfer the rebound is independent of the gas amount inside the bubble. Then the rebound becomes stronger because there is no energy consumed by the mass transfer.
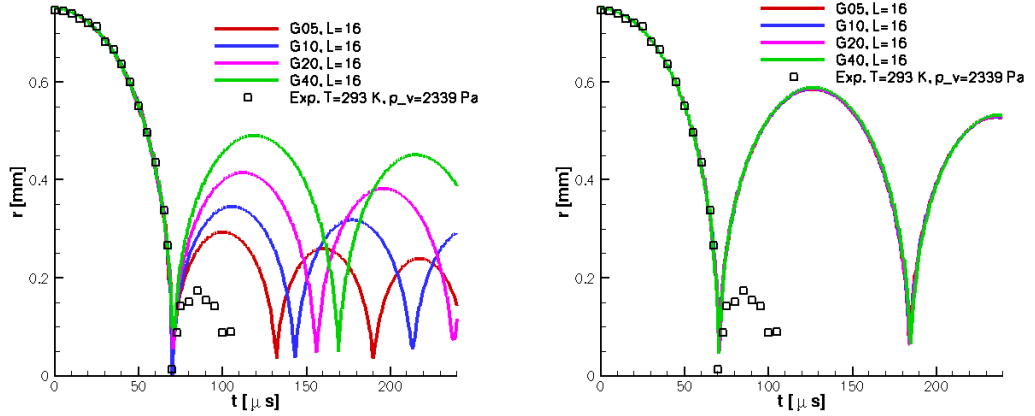
Figure 3: Bubble radius identified by $\alpha_{water} = 0.5$ versus time for computations with $L = 16$. Computation with (left) and without (right) mass transfer.

Temperature and gas volume fraction. In addition to the information of the bubble radius our computations provide information on the spatial distribution of the bubble state. Exemplarily we present in Figures 4 – 7 the temperature field and the field of the gas volume fraction, respectively, for both with and without mass transfer. Note that these plots are composed of the respective data extracted from the computations in the spatial interval [0,0.8] μm at every 24000 time step. We observe that in the first collapse the bubble state changes almost homogeneously in time and, thus, justifies the frequently made assumption in simplified models. However, in the rebound the bubble state becomes heterogeneous also in space due to the high compression of the bubble in the collapse and the acceleration of the interface causing a shock wave in the gas that is emanating into the liquid. Furthermore we observe that the highest temperatures reached in the first collapse stay within a reasonable range. In particular, the maximal temperature increases with the amount of gas inside the bubble as expected. Typically the maximal temperatures are smaller when taking mass transfer into account due

(a) G05: Temperature

(b) G05: Temperature

(c) G05: Gas volume fraction
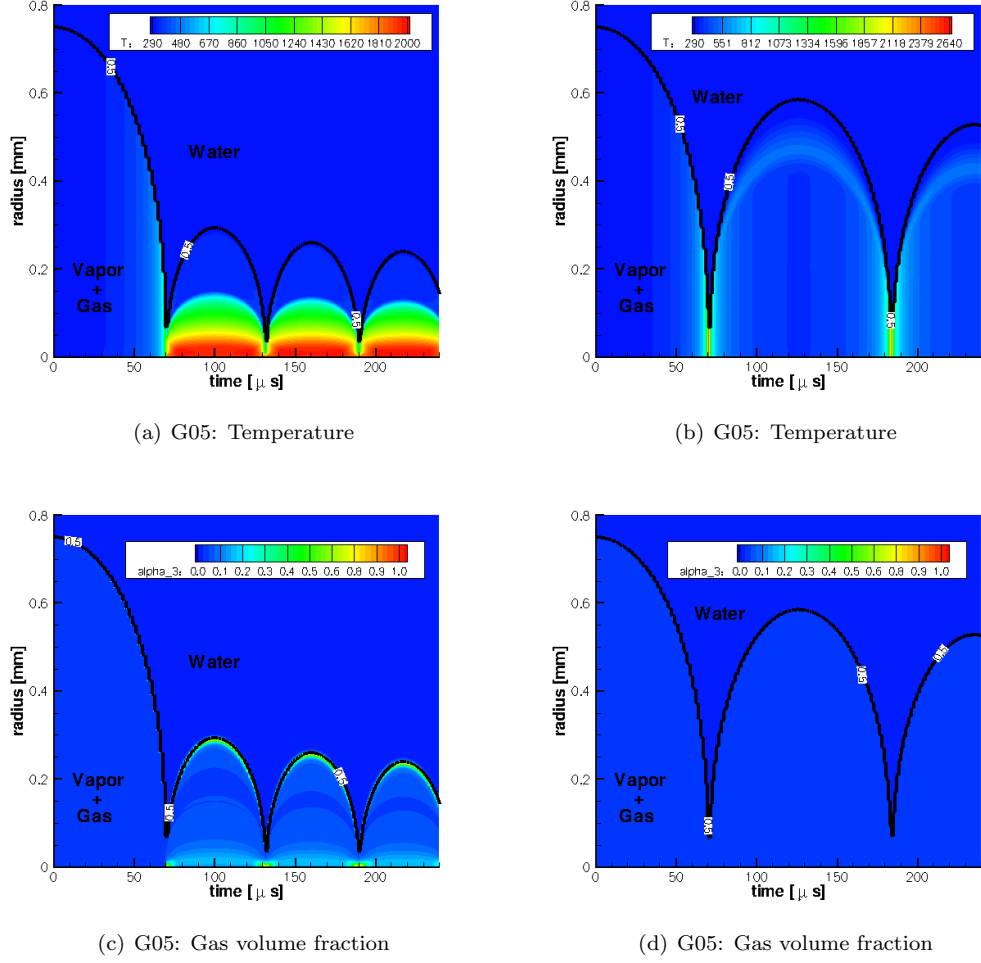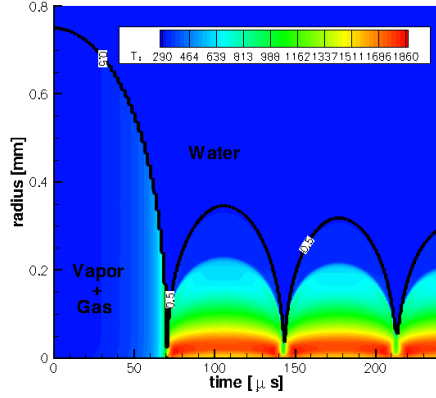

(d) G05: Gas volume fraction

Figure 4: Case G05: Temperature and gas volume fraction for computations with (left) and without (right) mass transfer. Bubble interface identified by $\alpha_{water} = 0.5$ for computations with $L = 16$.

to the energy consumption in the phase change. Note that the temperature typically becomes unphysically high in the collapse if no temperature relaxation is performed and, thus, is in general not presented.

For the gas volume fraction we observe that it is not varying in the first collapse but remains almost constant until the collapse. In the rebound we observe a higher concentration of gas near the interface when taking mass transfer into account. Note that the interface is impermeable for the gas because mass transfer is only accounted for between water vapor and liquid water. Opposite to this, the gas volume fraction remains almost homogeneous without mass transfer. Finally, we emphasize that the interface is not smeared in contrast to computations that have been performed with the stiffened gas approach by Saurel-Abgrall [38] presented in [33].

Grid convergence. In order to investigate the influence of the resolution on the numerical results we perform additional computations using lower resolutions corresponding to $L = 13, 14, 15$ refinement levels. The corresponding numbers of cells on a uniformly refined grid in the computational domain and inside the initial bubble of radius $r_I = R_{max}$ are listed in Table 5. In Figures 8 and 9 we present the bubble radius for different resolution levels for all four cases. In the first rebound there is no difference visible, i.e., this part seems to be grid converged. However, in the following bubble oscillations we note that the rebound becomes more pronounced with increasing refinement level and, thus, the collapse times increase. There were
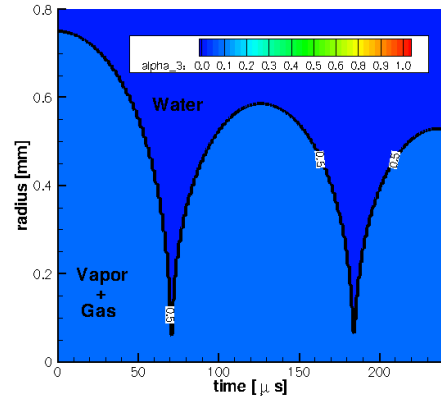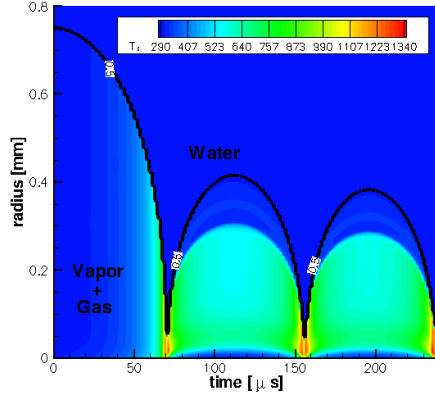
(a) G10: Temperature
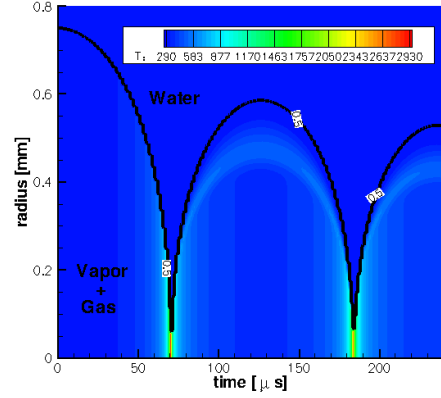
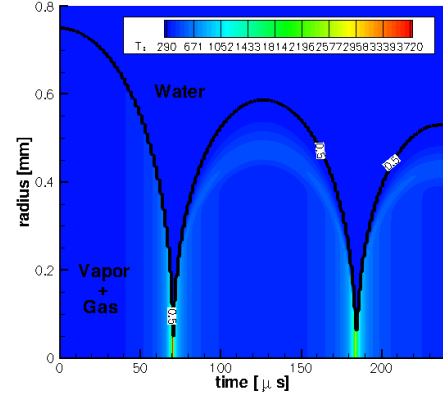(b) G10: Temperature
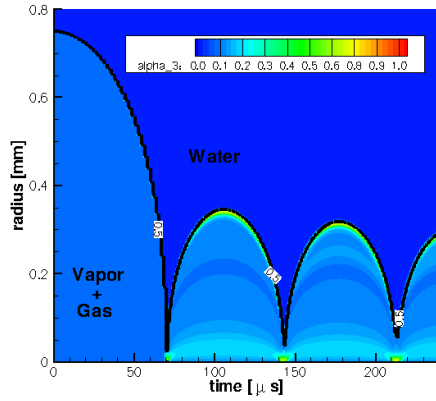
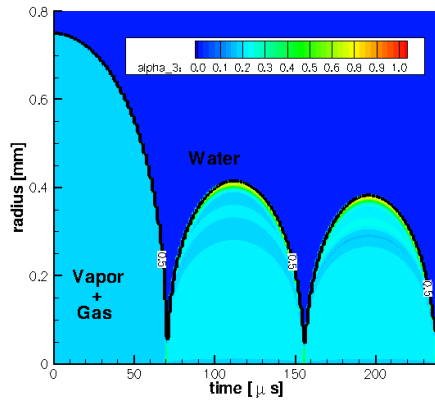(c) G10: Gas volume fraction

(d) G10: Gas volume fraction

Figure 5: Case G10: Temperature and gas volume fraction for computations with (left) and without (right) mass transfer. Bubble interface identified by $\alpha_{water} = 0.5$ for computations with $L = 16$.
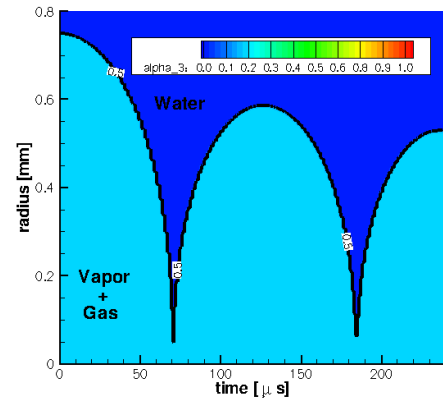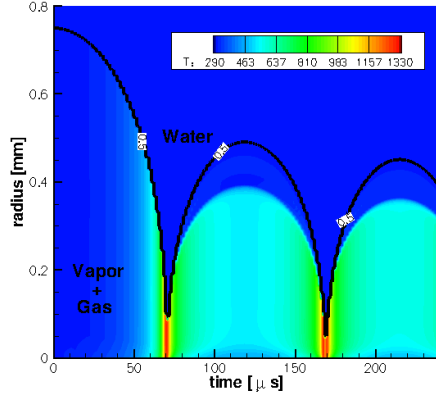
(a) G20: Temperature

(b) G20: Temperature
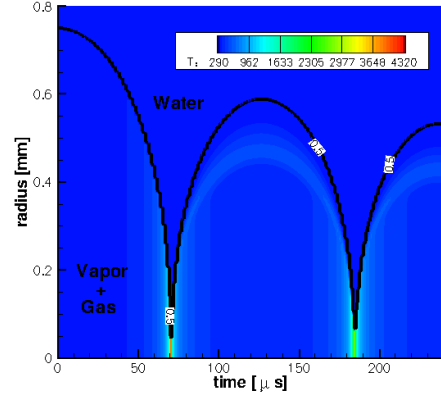
(c) G20: Gas volume fraction
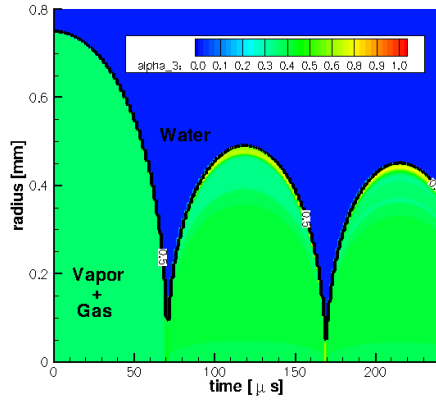
(d) G20: Gas volume fraction

Figure 6: Case G20: Temperature and gas volume fraction for computations with (left) and without (right) mass transfer. Bubble interface identified by $\alpha_{water} = 0.5$ for computations with $L = 16$.
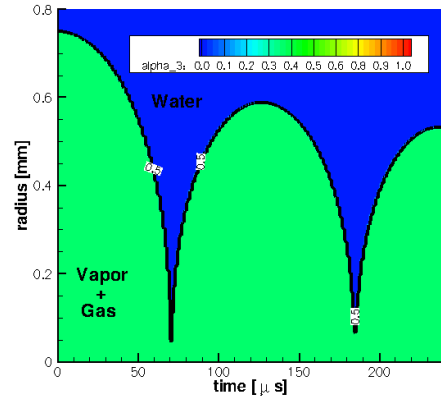
(a) G40: Temperature

(b) G40: Temperature

(c) G40: Gas volume fraction

(d) G40: Gas volume fraction

Figure 7: Case G40: Temperature and gas volume fraction for computations with (left) and without (right) mass transfer. Bubble interface identified by $\alpha_{water} = 0.5$ for computations with $L = 16$.

L	13	14	15	16
N_L	131072	262144	524288	1048576
$N_{I,L}$	256	512	1024	2048

Table 5: Number of cells on uniformly refined grid (N_L) and number of cells inside initial bubble ($N_{I,L}$) for different number of refinement levels (L).

similar findings reported in [48]. Thus the solution seems not yet to be grid converged.

One reason might be that viscosity and heat conduction have been neglected in the multi-component model. In our computations we observe that with finer resolution the maximal pressure and temperature states inside the bubble are increasing. A similar observation was made by Guderley in case of the focusing of spherical shock waves, see [19]. His asymptotic analysis predicts infinite states when the shock focuses in the center for the inviscid case but these remain bounded taking into account viscosity and heat conduction. This was later on confirmed numerically, see [21].

Another reason might be that in our model we do not account for the interaction of different components due to velocity and inertia. This is only justified for small velocities, see [13], p. 146. However, in the collapse the phase interface is significantly accelerated. For the same reason, the equilibrium assumption of the mass transfer is questionable. Condensation and vaporization will proceed on different time scales and should therefore be modeled in non-equilibrium.

Remark. Finally we would like to comment on similar results presented in [48]. There a reduced three-component model is used where only *one* velocity for all phases is taken into account. Although less equations had to be solved and the computational domain [0,0.099] m has been much smaller, the computational costs are much higher due to iterations involved in the relaxation procedures as discussed in Section 3.3 and performing the computations on uniform grids. Computational times were in the order of 1000 CPU hours on the system 4 core AMD Opteron(tm) 2218, 2.6 GHz, 32 GB Ram.

Due to local grid adaptation applied in our computations the number of cells in the locally refined grids is by several orders smaller than the one used for the computations presented in [48] although the fully refined grids corresponding to $L = 13$, 14, 15 provide the same resolution as in [48] corresponding to the computations with $N_I = 250$, 500, 1000, see Table 5 and 6. Therefore our computations that have been performed on the system 84 core AMD Opteron 8356, 2.3 GHz, 256 GB Ram took at most 60 CPU hours. This is a tremendous speedup in comparison to [48]. Furthermore, in [48] only two components have been relaxed and the third component has been determined by the saturation constraint (1). This may cause unphysical production of energy and momentum.

L	13	14	15	16
G05	1517	1720	2102	3024
G10	1480	1719	2193	3079
G20	1422	1655	2237	2889
G40	1352	1624	2123	2924

| L	13	14	15	16
G05	1176	1591	2020	2844
G10	1179	1551	2032	2736
G20	1182	1584	2083	2632
G40	1188	1577	1998	2624

Table 6: Maximal number of cells on locally refined grid for different number of refinement levels L. Computations with (left) and without (right) mass transfer.

4.3   Shock-bubble interaction

For a multi-dimensional application we consider the interaction of a collapsing bubble with a planar shock wave. This problem is important for medical applications such as shock wave lithotripsy, as well as from a more fundamental point of view because bubbles in a cloud are exposed to the collapse shock waves of neighboring bubbles. This problem has been investigated both by so-called lithotripter shock wave (LSW) experiments and numerical simulations. For
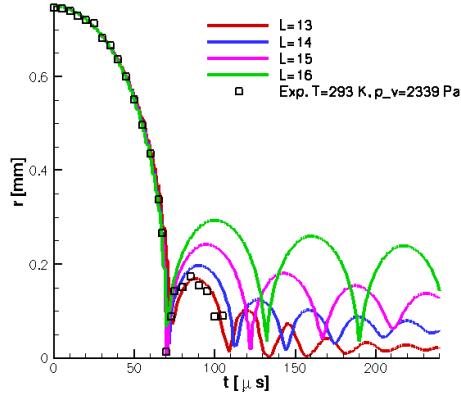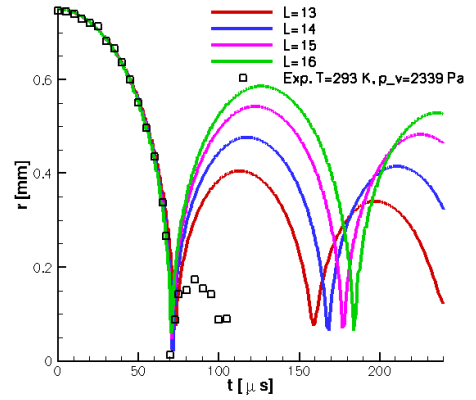
(a) G05
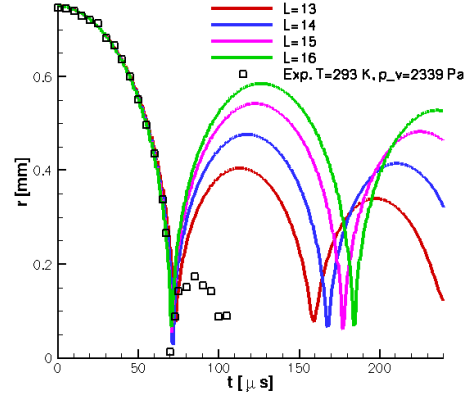
(b) G05
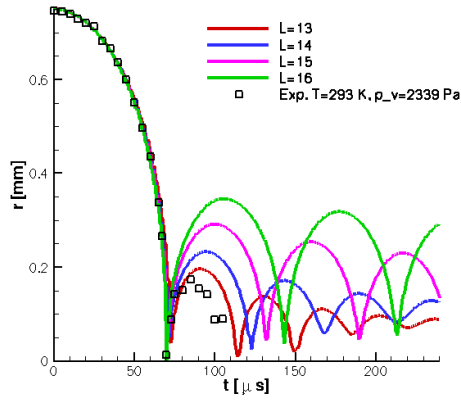
(c) G10

(d) G10

Figure 8: Bubble radius identified by $\alpha_{water} = 0.5$ versus time for different number of refinement levels. Computations with (left) and without (right) mass transfer.
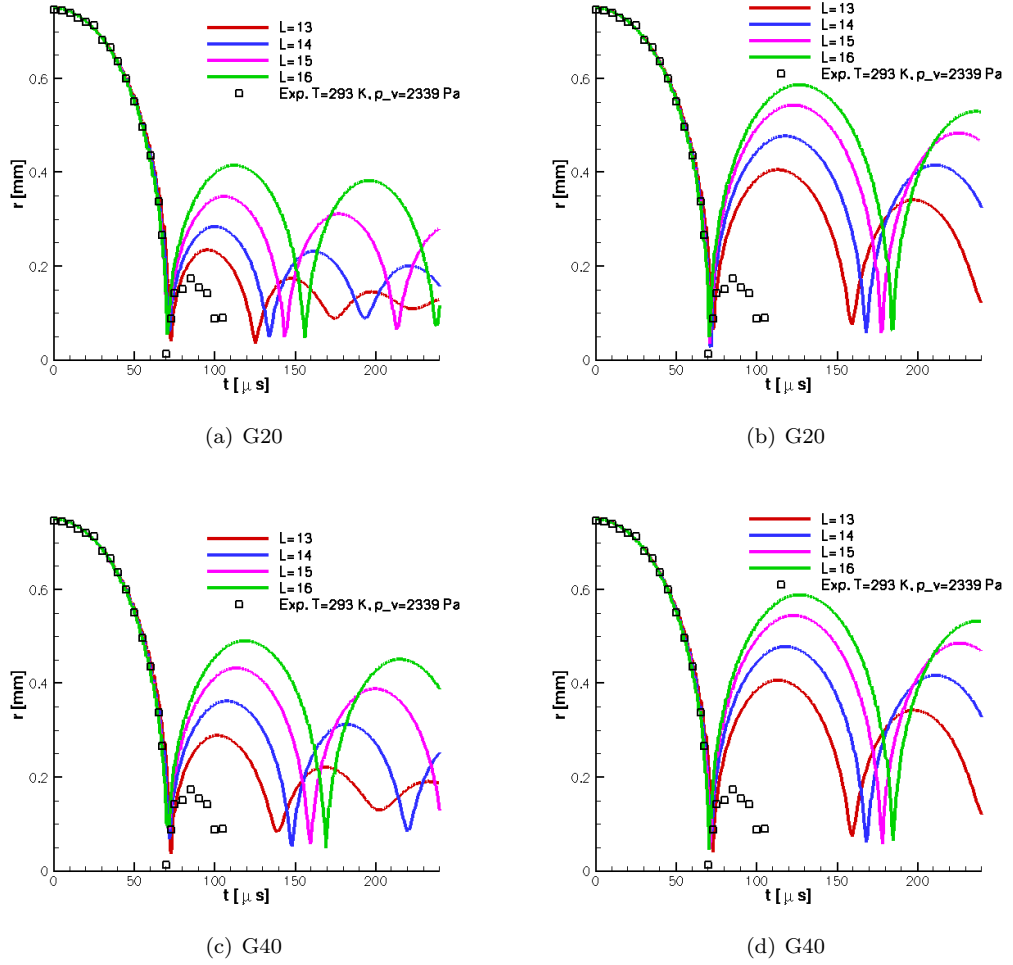
Figure 9: Bubble radius identified by $\alpha_{water} = 0.5$ versus time for different number of refinement levels. Computations with (left) and without (right) mass transfer.
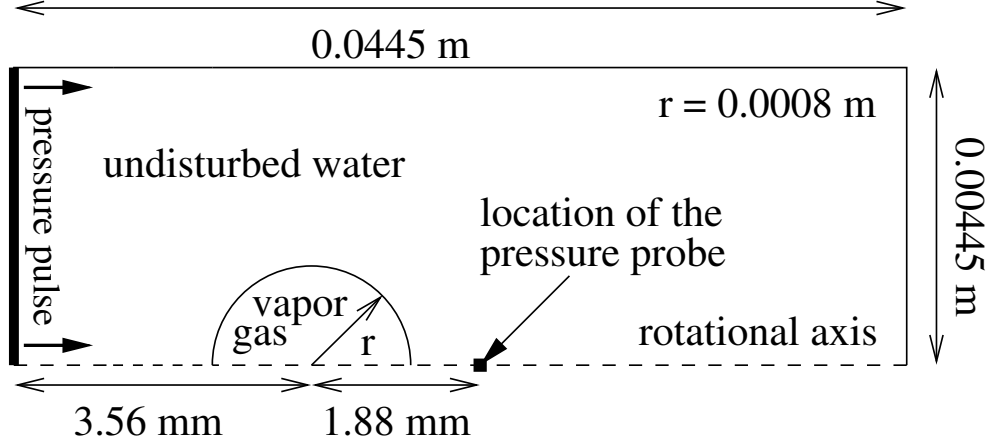
Figure 10: Computational setup.

		S_b	S_0	S_p
p	$[Pa]$	2339	1×10^5	8×10^7
T	$[K]$	293	293	293
$\boldsymbol{v}$	$[m/s]$	$\mathbf{0}$	$\mathbf{0}$	$\mathbf{0}$
α_{vapor}		$0.1 - \epsilon_2$	ϵ_1	ϵ_1
α_{water}		ϵ_2	$1 - 2\epsilon_1$	$1 - 2\epsilon_1$
α_{gas}		0.9	ϵ_1	ϵ_1

Table 7: Initial data with $\epsilon_1 = 10^{-4}$ and $\epsilon_2 = 10^{-8}$. The state inside the bubble S_b, the ambient water state S_0 and the pressure pulse S_p are assumed to be in equilibrium.

a detailed review we refer to [1, 4] and references cited therein. Since in this paper the main objective is on the feasibility of multi-dimensional multi-component simulations the focus is on the numerical simulation rather than the comparison with experiments, we therefore confine ourselves to a simplified quasi-two-dimensional computational setting employing rotational symmetry as sketched in Figure 10.

Computational setup. The computation is initialized with a bubble of radius 0.8 mm filled with liquid vapor and non-condensable gas. Since the state inside the bubble cannot be observed experimentally, we assume that the state is homogeneous and at rest with pressure 2339 Pa and temperature 293 K referred to as state S_b. The bubble is embedded in water at rest where the ambient state S_0 is determined by the pressure 1 bar and the temperature 293 K. The computation is first started without perturbation in the water. Then at time $T_0 = 37.45 \, \mu s$ a pressure pulse with pressure condition S_p of 80 MPa starts propagating from the left boundary. The pressure pulse lasts $0.23 \, \mu s$ before recovering the initial water state at rest S_0. The boundary conditions at the left boundary are thus given by

$$S(t) = \begin{cases} S_0, & t < T_0 \text{ or } t > T_1 \\ S_p, & T_0 \leq t \leq T_1 \end{cases} \tag{130}$$

with $T_1 = 37.68 \, \mu s$. The initial conditions are recorded in Table 7.

Discretization. Since the problem is inherently two-dimensional due to rotational symmetry, we perform quasi-two-dimensional computations where we have to take the change of metric into account in the fluid discretization (56) and (57). For a structured grid in a two-dimensional space with longitudinal coordinate z and radial coordinate r, i.e., $V_{\boldsymbol{i}} = [z_{i-\frac{1}{2}}, z_{i+\frac{1}{2}}] \times [r_{j-\frac{1}{2}}, r_{j+\frac{1}{2}}]$

with $\boldsymbol{i} = (i,j)$, the resulting scheme can be written as

$$(\alpha_k)_{\boldsymbol{i}}^{n+1} \;=\; (\alpha_k)_{\boldsymbol{i}}^n - \frac{\Delta t}{\|V_{\boldsymbol{i}}\|} \sum_{\boldsymbol{j} \in \mathcal{N}(\boldsymbol{i})} \|\Gamma_{\boldsymbol{ij}}\| \, (\overline{\boldsymbol{V}}_I)_{\boldsymbol{ij}} \cdot (\nabla \alpha_k)_{\boldsymbol{ij}}^n, \tag{131}$$

$$(\boldsymbol{u}_k)_{\boldsymbol{i}}^{n+1} \;=\; (\boldsymbol{u}_k)_{\boldsymbol{i}}^n - \frac{\Delta t}{\|V_{\boldsymbol{i}}\|} \sum_{\boldsymbol{j} \in \mathcal{N}(\boldsymbol{i})} \|\Gamma_{\boldsymbol{ij}}\| \, \boldsymbol{G}_{\boldsymbol{ij}}^n + \frac{\Delta t |V_{ij}|}{\|V_{ij}\|} \boldsymbol{S}_{ij}^n, \tag{132}$$

with the volumes $|V_{(i,j)}| := \Delta z_i \, \Delta r_j = (z_{i+\frac{1}{2}} - z_{i-\frac{1}{2}})(r_{j+\frac{1}{2}} - r_{j-\frac{1}{2}})$, $\|V_{(ij)}\| := r_j \Delta r_j \Delta z_i$, $r_j := (r_{j+\frac{1}{2}} + r_{j-\frac{1}{2}})/2$ and the interface areas $\|\Gamma_{(i,j),(i,j\pm1)}\| := \Delta z_i \, r_{j\pm\frac{1}{2}}$ and $\|\Gamma_{(i,j),(i\pm1,j)}\| := r_j \, \Delta r_j$. Since in each time step pressure is at equilibrium, we employ here the identity (51), i.e., the fluxes and the derivatives of the volume fractions are given by (60) and (59), respectively. Here the fluxes and the derivatives of the volume fractions are given by (58) and (59), respectively. Note that $\boldsymbol{u}_k = \alpha_k(\rho_k, \rho_k(v_z)_k, \rho_k(v_r)_k, E_k)^T$ is now composed of the density, the momentum in longitudinal and radial direction and total energy of component k. The additional metric term is defined by $\boldsymbol{S}_k(\boldsymbol{w}) = (0, \alpha_k p_k, 0, 0)^T$. This quasi-two-dimensional scheme can be derived from the three-dimensional discretization applied to a special grid similar to [6] and, in more details, in [4], Appendix A. For our problem we choose the computational domain as $\Omega = [0, 0.0445] \times [0, 0.00445]$ m^2 to avoid unphysical reflections from the right boundary and a short distance between the pressure pulse and the bubble at the left boundary. The domain is discretized by 50×5 cells on the coarsest level using $L = 7$ refinement levels. The threshold value is chosen as $\epsilon_{thresh} = 10^{-3}$. We perform 120000 time steps with CFL number 0.5. The computation is performed with mass transfer.

Numerical results. The initial phase of the computation is characterized by a rarefaction wave and a shock wave both emanating from the bubble interface and running into the liquid and towards the bubble center, respectively, see Fig. 11(a). The shock wave is focusing in the bubble center where it is reflected. The reflected shock wave is then interacting with the bubble interface where it is partially transmitted into the liquid and partially reflected. Thus the shock wave is bouncing between the bubble center and the bubble interface. Due to the interactions the bubble starts shrinking.

The second phase starts at time $t = T_0$ where the pressure pulse enters the computational domain at the left boundary, see Fig. 11(b). It hits the bubble at about $t = 39.5$ μs with the bubble at a radius of approximately 0.59 mm, see Fig. 12. The LSW is partially transmitted and reflected at the interface, see Figs. 11(c) and 11(d). The reflected LSW causes a significant pressure drop in the water causing vaporization, see Fig. 11(e). With advancing time the pressure raises again and the vapor condensates again causing pressure waves, see Fig. 11(f).

In a final phase the bubble interface is significantly accelerated due to the interaction with the LSW and the bubble collapses, see Fig. 11(f). When the bubble collapses at about $t = 44.32$ μs shock waves are emanated into the liquid, see Fig. 12.

An overview of the wave dynamics is given in Fig. 12 where we extract data on the symmetry axis every 50 time steps. The pressure gradient magnitude shows very well the collapse of the bubble and the emanated shock waves.

Finally we present in Fig. 13 a pressure probe taken on the symmetry axis at a distance of 1.88 mm behind the initial bubble center, see probe location in Fig. 10. The first peak is the pressure measurement of the LSW and the second one is shock-induced by the collapse.

5   Conclusion

A generalized multi-component fluid model has been introduced. This model is thermodynamically consistent as proven in [20]. It accounts for relaxation of velocity, pressure, temperature, and chemical potentials.

Opposite to former work, cf. [47, 34], pressure and temperature are relaxed simultaneously. Typically pressure relaxation relies on an approximation process that can cause numerical instabilities in case of strong pressure non-equilibrium, cf. [26]. Alternatively, iterative procedures can be used that make computations very expensive, in particular in multi dimensions. This is avoided in our pressure-temperature relaxation procedure. In particular, we have proven that an equilibrium state always exists such that the equilibrium temperature as well as the

(a) 3.50 μs

(b) 38.74 μs

(c) 39.80 μs

(d) 40.80 μs

(e) 44.39 μs

(f) 45.40 μs

Figure 11: Pressure gradient magnitude with bubble interface IF identified by $\alpha_{water} = 0.5$, rarefaction wave RW, lithotripter shock wave LSW, vaporization region V and collapse shock CS.
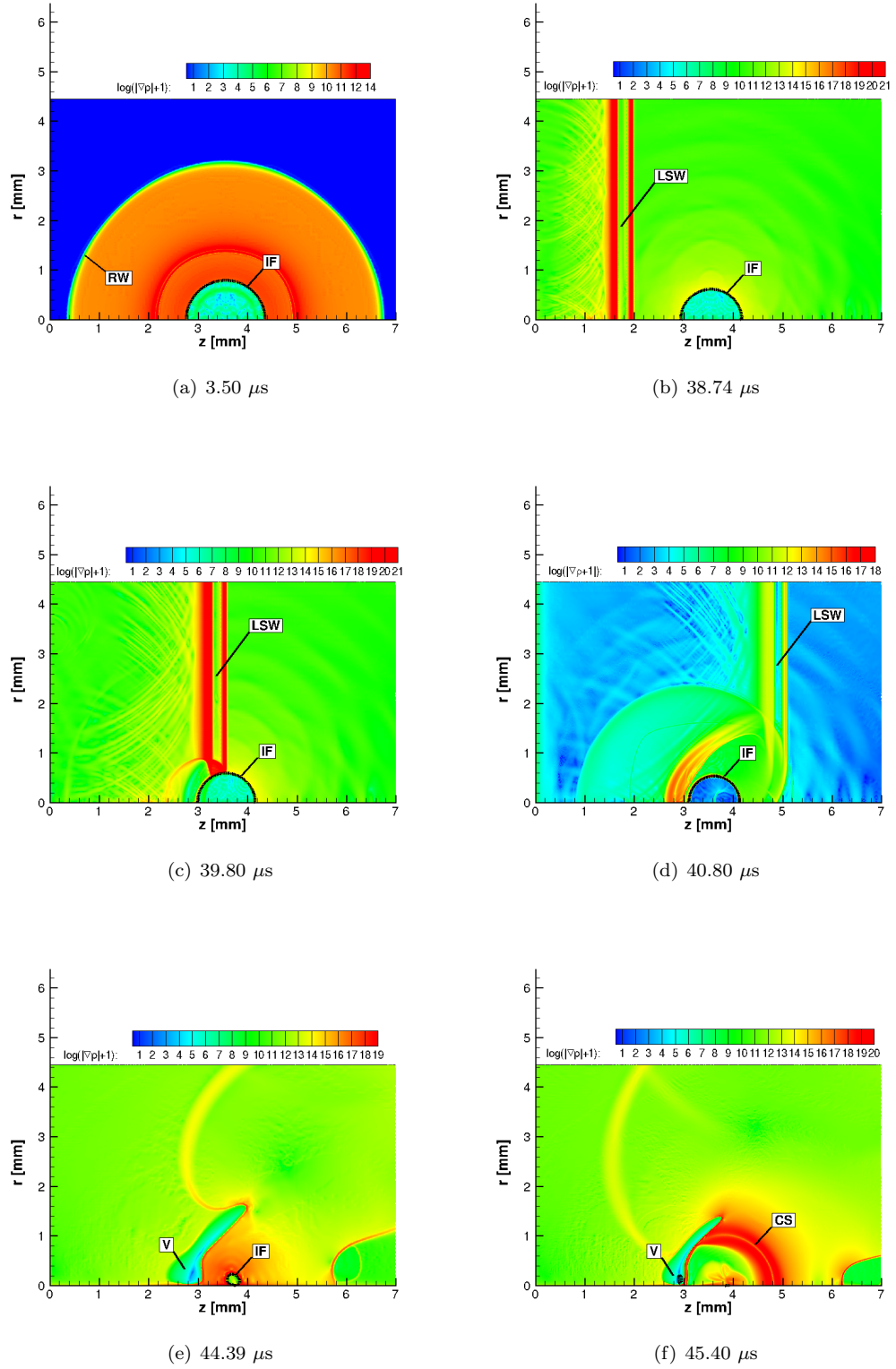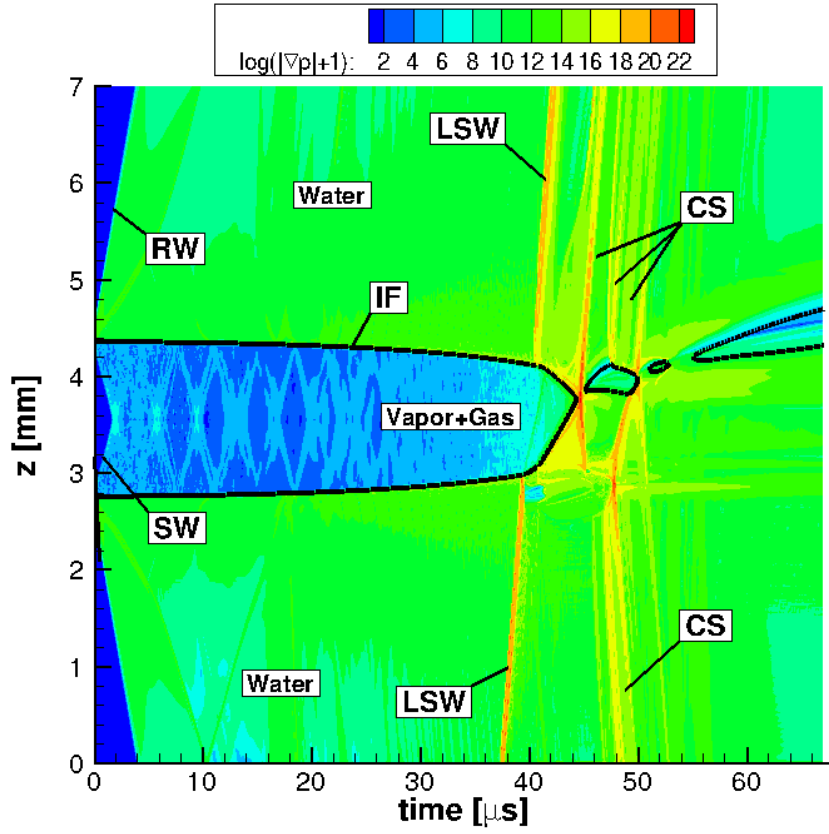
Figure 12: Pressure gradient magnitude with bubble interface IF identified by $\alpha_{water} = 0.5$, rarefaction wave RW, shock wave SW, lithotripter shock wave LSW and collapsing shock waves CS.
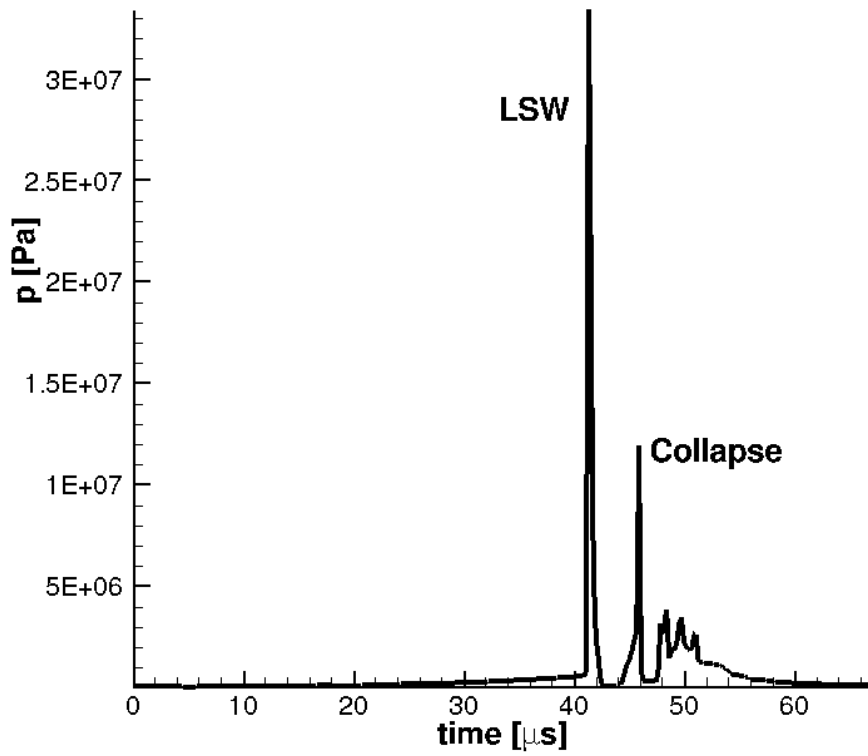

Figure 13: Pressure probe.

equilibrium pressure are positive and the volume fractions are in the admissible range. This proof applies for an arbitrary number of components.

Instead of relaxing Gibbs free energies as in [48] we perform relaxation of the chemical potentials in case of three or more components. Exemplarily for a three-component model consisting of water vapor, liquid water and inert gas we have verified that either a unique equilibrium state exists or one phase vanishes. This model is consistent with the two-component model if the inert gas is not present. We emphasize that determining the equilibrium state only requires a single iteration procedure whereas in [48] an additional internal iteration is needed. This significantly speeds up the computation.

This model is solved numerically by applying an operator splitting where the evolution of the fluid and the relaxation to equilibrium are separated in each time step. For the solution of the homogenized fluid equations we apply a second order finite volume solver based on ENO reconstruction and the HLLC Riemann solver. Computations are performed on a locally refined grid where grid adaptation is triggered by advanced multi-scale techniques, cf. [31, 32]. We emphasize that local grid adaptation is a key ingredient to perform the computations in affordable time. Moreover, we apply thermal and chemical relaxation throughout the computational domain instead of an artificial interface region near the phase boundary as done for instance in [34, 48].

Stability and efficiency of the model and the implementation are verified by means of a spherical symmetric collapse of a laser induced cavitation bubble as well as a two-dimensional shock-bubble interaction for a three-component fluid.

Quasi-one-dimensional numerical simulations of a collapsing bubble filled with non-condensable gas and condensable water vapor in liquid water are performed for varying amount of non-condensable gas. The computations show a strong effect on the rebound with increasing amount of non-condensable gas. However, the rebound is grid-dependent, i.e., the rebound increases under grid refinement. This indicates that some physical effect is still missing in the model. The asymptotic analysis of Guderley [19] for the collapse of a spherical shock wave in a single-phase fluid indicates that viscosity and heat conduction might be accounted for. This is in agreement with the findings in [10]. In addition, the phase transition might be modeled in non-equilibrium because of the very high speeds of the phase interface in the collapse.

In order to verify that also multi-dimensional computations are feasible for the model at hand we have considered the interaction of a collapsing bubble with a planar shock wave. This problem is important for medical applications such as shock wave lithotripsy. To our knowledge this is one of the first 2d-computations presented using this type of model besides the two-component simulations in [34]. However, we emphasize that our computations are more complex due to three components and taking into account also chemical potentials, but are more efficient due to grid adaptation and the improved relaxation procedures.

References

[1] M. Alizadeh, Experimental investigation of shock wave-bubble interaction, Phd thesis, Drittes Physikalisches Institut, Göttingen, 2010.

[2] N. Andrianov, Analytical and numerical investigation of two-phase flows, PhD thesis, Otto-von-Guericke University, Magdeburg, 2003.

[3] N. Andrianov, R. Saurel, G. Warnecke, A simple method for compressible multiphase mixtures and interfaces, Int. J. Numer. Meth. Fluids, 41 (2003), 109–131.

[4] M. Bachmann, Dynamics of cavitation bubbles in compressible two-phase fluid flow, PhD thesis, RWTH Aachen, `http://darwin.bth.rwth-aachen.de/opus3/volltexte/2013/4554/pdf/4554.pdf`, 2013.

[5] M.R. Baer, J.W. Nunziato, A two-phase mixture theory of the deflagration-to-detonation transition (DDT) in reactive granular materials, Int. J. Multiphase Flows, 12 (1986), 861–889.

[6] T. Barberon, Ph. Helluy, S. Rouy, Practical computation of axisymmetrical multifluid flows, International Journal of Finite Volumes, 1(1) (2003), 1–34.

[7] R.A. Berry, R. Saurel, F. Petitpas, A simple and efficient diffuse interface method for compressible two-phase flows, 2009 International Conference on Mathematics, Computational Methods & Reactor Physics, Preprint, 2009.

[8] J. Dalton, A new System of Chemical Philosophy, 3 vols, Manchester 1808.

[9] J. Dalton, A new System of Chemical Philosophy, in: Ostwalds Klassiker der Exacten Wissenschaften, Band 3, Leipzig 1889.

[10] W. Dreyer, F. Duderstadt, M. Hantke, G. Warnecke, Bubbles in liquids with phase transition. Part 1: On phase change of a single vapor bubble in liquid water, Continuum Mechanics and Thermodynamics, 24 (2012), 461–483.

[11] S.F. Davis, Simplified second-order Godunov-type methods, SIAM J. Sci. Stat. Comput., 9(3) (1988), 445–473.

[12] D. Drew, Mathematical modeling of two-phase flow, Ann. Rev. Fluid Mech., 15 (1983), 261–291.

[13] D.A. Drew, S.L. Passman, Theory of Multicomponent Fluids, Applied Mathematical Sciences, Vol. 135, Springer, 1999.

[14] I. Eick, Experimentelle und numerische Untersuchungen zur Dynamik sphährischer und asphährischer Kavitationsblasen, PhD thesis, University of Darmstadt, 1992.

[15] P. Embid, M. Baer, Mathematical analysis of a two-phase continuum mixture theory, Contin. Mech. Thermodyn., 4 (1992), 279–312.

[16] T. Flåtten, H. Lund, Relaxation two-phase flow models and the subcharacteristic condition, Preprint Sintef, Norway, 2011.

[17] T. Gallouët, J.-M. Herard, N. Seguin, Numerical modelling of two-phase flows using the two-fluid two-pressure approach, Math. Models Methods Appl. Sci., 14(5) (2004), 663–700.

[18] F.R. Gilmore, The growth or collapse of a spherical bubble in a viscous compressible liquid, Report No 26-4 Hydrodynamics Laboratory, California Institute of Technology, Pasadena, California, USA, 1952.

[19] G. Guderley, Starke kugelige und zylindrische Verdichtungsstöße in der Nähe des Kugelmittelpunktes bzw. der Zylinderachse, Luftfahrtforschung, 19 (1942), 302–312.

[20] E. Han, M. Hantke, S. Müller, Some remarks on the closure of non-equilibrium multi-component models, Preprint, in preparation.

[21] M. Hanke, J. Ballmann, Strong Changes of State in Collapsing Bubbles, ZAMM, 78(Suppl. 1) (1998), 453–454.

[22] F. Harlow, A. Amsden, Fluid dynamics, Technical Report, LA-4700, Los Alamos National Laboratory, 1971.

[23] J.-M. Herard, A three-phase flow model, Mathematical and Computer Modelling, 45 (2007), 732–755.

[24] A. Kapila, R. Menikoff, J. Bdzil, S. Son, D. Stewart, Two-phase modelling of DDT in granular materials: Reduced equations, Phys. Fluid, 13 (2001), 3002–3024.

[25] J.B. Keller, M. Miksis, Bubble oscillations of large amplitude, J. Acoust. Soc. Am., 68(2) (1980), 628–633.

[26] M.H. Lallemand, A. Cinnayya, O. Le Metayer, Pressure relaxation procedures for multiphase compressible flows, Int. J. Numer. Meth. Fluids, 49(1) (2005), 1–56.

[27] W. Lauterborn, Th. Kurz, Physics of bubble oscillations, Rep. Prog. Phys., 73 (2010), 106501.

[28] T.-P. Liu, Hyperbolic conservation laws with relaxation, Commun. Math. Phys, 108 (1987), 153–175.

[29] I. Müller, Thermodynamics, Pitman, London, 1985.

[30] I. Müller, W. Müller, Fundamentals of Thermodynamics and Applications, Springer-Verlag, Berlin, 2009.

[31] S. Müller, Adaptive multiscale schemes for conservation laws, Lecture Notes in Computational Science and Engineering, 27, Berlin: Springer, 2003.

[32] S. Müller, Multiresolution schemes for conservation laws, R. DeVore, A. Kunoth (eds.), Multiscale, nonlinear and adaptive approximation. Dedicated to Wolfgang Dahmen on the occasion of his 60th birthday. Berlin: Springer, 379–408, 2009.

[33] S. Müller, M. Bachmann, Ph. Helluy D. Kröninger, Th. Kurz, Comparison and validation of compressible flow simulations of laser-induced cavitation bubbles, Computers & Fluids, 38 2009, 1850–1862.

[34] M. Pelanti, K.-M. Shyue. A mixture-energy-consistent six-equation two-phase numerical model for fluids with interfaces, cavitation and evaporation waves, J. Comput. Phys., 259 (2014), 331–357.

[35] Lord Rayleigh, On the pressure developed in a liquid during the collapse of a spherical cavity, Phil. Mag. Ser., 34(6) (1917), 94–98.

[36] K. Saleh, Analyse et Simulation Numérique par Relaxation d'Écoulements Diphasiques Compressibles, PhD thesis, Université Pierre et Marie Curie, Paris, 2012.

[37] R. Saurel, R. Abgrall, A multiphase Godunov method for compressible multifluid and multiphase flows, J. Comput. Phys., 150(2) (1999), 425–467.

[38] R. Saurel, R. Abgrall, A simple method for compressible multifluid flows, SIAM J. Sci. Comput., **21**, No. 3 (1999), 1115-1145.

[39] R. Saurel, O. LeMetayer, A multiphase flow model for compressible flows with interfaces, shocks, detonation waves and cavitation, J. Fluid Mech., 43 (2001), 239–271.

[40] R. Saurel, F. Petitpas, R. Abgrall, Modelling phase transition in metastable liquids: Application to cavitation and flashing flows, J. Fluid. Mech., 607 (2008), 313–350.

[41] H. Söhnholz, Th. Kurz, Thermal Effects upon Collapse of Laser-induced Cavitation Bubbles, DOI:10.3850/978-981-07-2826-7_137, Proceedings of 8th International Symposium on Cavitation, Singapore, 13–16 August 2012.

[42] U. Specht, Numerical Simulation of Mechanical Waves at Fluid-Solid-Interfaces, PhD thesis, RWTH Aachen, 2000 (in German).

[43] G. Strang, On the construction and comparison of difference schemes, SIAM J. Numer. Anal., 5 (1968) 506-517.

[44] M. Tinguely, The effect of pressure gradient on the collapse of cavitation bubbles in normal and reduced gravity, PhD thesis, École Polytechnique Fédérale de Lausanne, 2013.

[45] E. F. Toro, Riemann solvers and numerical methods for fluid dynamics: A practical introduction, Berlin: Springer, 1997.

[46] A. Zein, Numerical methods for multiphase mixture conservation laws with phase transition, PhD thesis, Otto-von-Guericke University, Magdeburg, 2010.

[47] A. Zein, M. Hantke, G. Warnecke, Modeling phase transition for compressible two-phase flows applied to metastable liquids, J. Comput. Phys., 229(8) (2010), 2964–2998.

[48] A. Zein, M. Hantke, G. Warnecke, On the Modelling and Simulation of a Laser-Induced Cavitation Bubble, Int. J. Num. Meth. Fluids., 73(2) (2013), 172-203.

A   Upwind discretization according to Saurel and Abgrall

For the discretization of the hyperbolic problem (52) and (53) we follow the Saurel-Abgrall approach [37]. Opposite to the original work, we derive it for a general multi-dimensional discretization as outlined in Section 3.1. The key idea is to design a discretization that preserves homogeneous pressure and velocity fields. For this purpose, we start with an arbitrary finite volume discretization for (52) that is in conservation form. For each phase $k = 1, \ldots, K$ it reads

$$
(\boldsymbol{u}_k)_i^{n+1} = (\boldsymbol{u}_k)_i^n \quad - \quad \frac{\Delta t}{|V_i|} \sum_{j \in \mathcal{N}(i)} |\Gamma_{ij}| \boldsymbol{F}_k(\boldsymbol{w}_{ij}^n, \boldsymbol{w}_{ji}^n, \boldsymbol{n}_{ij})
$$
$$
- \quad \Delta t \sum_{l=1,\neq k}^{K} \boldsymbol{H}_{k,l}(\boldsymbol{w}_i^n) (\nabla \alpha_l)_i^n, \tag{133}
$$

where we use the notation introduced in Section 3. Note that these discrete evolution equations are coupled by the numerical fluxes $\boldsymbol{F}_k$ that depend on the mass fractions and conserved quantities of *all* phases. The numerical fluxes in normal direction $\boldsymbol{n}$ are chosen arbitrarily but are assumed to satisfy the following consistency conditions

$$
\boldsymbol{F}_k(\boldsymbol{w}, \boldsymbol{w}, \boldsymbol{n}) = \sum_{i=1}^{d} \boldsymbol{f}_{k,i}(\alpha_k, \boldsymbol{u}_k) n_i, \ \forall \, \boldsymbol{w} = (\boldsymbol{\alpha}^T, \boldsymbol{u}_1^T, \ldots, \boldsymbol{u}_K^T)^T, \tag{134}
$$

$$
\sum_{j \in \mathcal{N}(i)} |\Gamma_{ij}| \, \boldsymbol{n}_{ij} = \boldsymbol{0}. \tag{135}
$$

Obviously, condition (134) holds if the numerical flux is computed by the original flux for an intermediate state determined by a Riemann solver, i.e.,

$$
\boldsymbol{F}_k(\boldsymbol{w}_L, \boldsymbol{w}_R, \boldsymbol{n}) = \sum_{i=1}^{d} \boldsymbol{f}_{k,i} \left((\alpha_k, \boldsymbol{u}_k)^*(\boldsymbol{w}_L, \boldsymbol{w}_R, \boldsymbol{n}) \right) n_i. \tag{136}
$$

The gradients $(\nabla \alpha_k)_i^n$ of the volume fractions are *not* yet determined. In order to derive an appropriate approximation of these terms we assume that at some time step n a homogeneous pressure and velocity field is given

$$
(p_k)_i^n = p, \quad (\boldsymbol{v}_k)_i^n = \boldsymbol{v}. \tag{137}
$$

In general the numerical fluxes involve the higher order reconstruction and the approximate solution of a Riemann problem. These are chosen such that they preserve homogeneous pressure and velocity fields. Therefore it is useful to apply the reconstruction to the primitive variables ρ_k, $\boldsymbol{v}_k$ and p_k instead of the conserved quantities of mass momentum and energy. Moreover, primitive reconstruction also preserves pressure and velocity equilibrium. We thus obtain for the homogeneous pressure and velocity fields

$$
(p_k)_{ij}^n = (p_k)_{ji}^n = p, \quad (\boldsymbol{v}_k)_{ij}^n = (\boldsymbol{v}_k)_{ji}^n = \boldsymbol{v} \ \text{(primitive reconstruction)} \tag{138}
$$
$$
(\bar{p}_k)_{ij}^n = (\bar{p}_k)_{ji}^n = p, \quad (\bar{\boldsymbol{v}}_k)_{ij}^n = (\bar{\boldsymbol{v}}_k)_{ji}^n = \boldsymbol{v} \ \text{(Riemann solver)} . \tag{139}
$$

Since we assume that in mechanical equilibrium the interfacial pressures and the interfacial velocity coincide with the equilibrium states, see equation (21), we also have

$$
(P_{k,l})_i^n = p, \quad (\boldsymbol{V}_I)_i^n = \boldsymbol{v} \ \text{(interfacial states)} . \tag{140}
$$

Then according to (136) the numerical flux $\boldsymbol{F}_k^n \equiv \boldsymbol{F}_k(\boldsymbol{w}_{ij}^n, \boldsymbol{w}_{ji}^n, \boldsymbol{n}_{ij})$ reads

$$
\boldsymbol{F}_k^n = (\bar{\alpha}_k \, \bar{\rho}_k \bar{v}_{kn})_{ij}^n \begin{pmatrix} 1 \\ (\bar{\boldsymbol{v}}_k)_{ij}^n \\ (\bar{E}_k)_{ij}^n + (\bar{p}_k)_{ij}^n/(\bar{\rho}_k)_{ij}^n \end{pmatrix} + (\bar{\alpha}_k)_{ij}^n \begin{pmatrix} 0 \\ (\bar{p}_k)_{ij}^n \boldsymbol{n}_{ij} \\ 0 \end{pmatrix} \tag{141}
$$

with the normal velocities $(\overline{v}_{kn})^n_{ij} := (\overline{\boldsymbol{v}}_k)^n_{ij} \cdot \boldsymbol{n}_{ij}$. Furthermore, the right-hand side in (133) simplifies due to the homogeneity of the interfacial pressures (140)

$$- \sum_{l=1,\neq k}^{K} \boldsymbol{H}_{k,l}(\boldsymbol{w}^n_i) (\nabla \alpha_l)^n_i = \boldsymbol{H}(\boldsymbol{w}^n_i) (\nabla \alpha_k)^n_i \quad \text{with} \quad \boldsymbol{H}(\boldsymbol{w}^n_i) := \begin{pmatrix} \boldsymbol{0}^T \\ P^n_i \boldsymbol{I}_{d\times d} \\ P^n_i ((\boldsymbol{V}_I)^n_i)^T \end{pmatrix}$$

see also equation (51), where we assume that the saturation condition (1) also holds on the discrete level.

¿From the homogeneity of velocity (139) we then deduce for the discrete density equation of phase k

$$(\alpha_k \rho_k)^{n+1}_i = (\alpha_k \rho_k)^n_i - \frac{\Delta t}{|V_i|} \sum_{j \in \mathcal{N}(i)} |\Gamma_{ij}| (\overline{\alpha}_k)^n_{ij} (\overline{\rho}_k)^n_{ij} v_{kn}. \tag{142}$$

Furthermore, for the discrete momentum equation of phase k we obtain by the homogeneity of pressure and velocity (139) and (140) as well as the discrete density equation (142)

$$(\alpha_k \rho_k \boldsymbol{v}_k)^{n+1}_i = \boldsymbol{v} (\alpha_k \rho_k)^{n+1}_i - p \left(\frac{\Delta t}{|V_i|} \sum_{j \in \mathcal{N}(i)} |\Gamma_{ij}| (\overline{\alpha}_k)^n_{ij} \boldsymbol{n}_{ij} - \Delta t (\nabla \alpha_k)^n_i \right). \tag{143}$$

In order to preserve the homogeneous velocity field at the new time step, i.e.,

$$(\boldsymbol{v}_k)^{n+1}_i = \boldsymbol{v}, \tag{144}$$

the last term has to vanish. This gives one equation for the approximation of the gradient of the volume fraction

$$(\nabla \alpha_k)^n_i = \frac{1}{|V_i|} \sum_{j \in \mathcal{N}(i)} |\Gamma_{ij}| (\overline{\alpha}_k)^n_{ij} \boldsymbol{n}_{ij} = \frac{1}{|V_i|} \sum_{j \in \mathcal{N}(i)} |\Gamma_{ij}| ((\overline{\alpha}_k)^n_{ij} - (\alpha_k)^n_i) \boldsymbol{n}_{ij}, \tag{145}$$

where in the last step we apply the geometric consistency (135) to point out the upwind character of the discretization. Next, we split the discrete energy into its internal and kinetic part, respectively,

$$(\alpha_k \rho_k \boldsymbol{v}^2_k)^{n+1}_i = (\alpha_k \rho_k \boldsymbol{v}^2_k)^n_i - \frac{\Delta t}{|V_i|} \sum_{j \in \mathcal{N}(i)} |\Gamma_{ij}| \overline{v}^n_{kn,ij} \left(\overline{(\alpha_k \rho_k \boldsymbol{v}^2_k)}^n_{ij} \right) \tag{146}$$

$$(\alpha_k \rho_k e_k)^{n+1}_i = (\alpha_k \rho_k e_k)^n_i - \frac{\Delta t}{|V_i|} \sum_{j \in \mathcal{N}(i)} |\Gamma_{ij}| (\overline{v}_{kn})^n_{ij} \left(\overline{(\alpha_k \rho_k e_k)}^n_{ij} + (\overline{\alpha}_k)^n_{ij} (\overline{p}_k)^n_{ij} \right)$$
$$+ \Delta t P^n_i \boldsymbol{V}^n_i \cdot (\nabla \alpha_k)^n_i \tag{147}$$

Again, from the homogeneity of pressure and velocity (139) and (140) as well as the discrete density equation (142) we conclude that by (144) the discrete kinetic energy is satisfied and by (145) the discrete energy equation simplifies to

$$(\alpha_k \rho_k e_k)^{n+1}_i = (\alpha_k \rho_k e_k)^n_i - \frac{\Delta t}{|V_i|} \sum_{j \in \mathcal{N}(i)} |\Gamma_{ij}| (\overline{v}_{kn})^n_{ij} (\overline{\alpha_k \rho_k e_k})^n_{ij}. \tag{148}$$

In case of the stiffened gas law (22) and the homogeneity of the pressure (139) we conclude

$$\rho_k (e_k - q_k) = \frac{p_k + \gamma_k \pi_k}{\gamma_k - 1} = \frac{p + \gamma_k \pi_k}{\gamma_k - 1} = const. \tag{149}$$

On the other hand, we may add a constant to the discrete energy equation (148), because of the geometric consistency (135)

$$(\alpha_k \rho_k (e_k - q_k))^{n+1}_i =$$
$$(\alpha_k \rho_k (e_k - q_k))^n_i - \frac{\Delta t}{|V_i|} \sum_{j \in \mathcal{N}(i)} |\Gamma_{ij}| (\overline{v}_{kn})^n_{ij} (\overline{\alpha_k \rho_k (e_k - q_k)})^n_{ij}. \tag{150}$$

Together with (149) we finally obtain the discrete evolution equation for the volume fraction

$$(\alpha_k)_i^{n+1} = (\alpha_k)_i^n - \frac{\Delta t}{|V_i|} \sum_{j \in \mathcal{N}(i)} |\Gamma_{ij}| (\overline{v}_{kn})_{ij}^n (\overline{\alpha}_k)_{ij}^n. \tag{151}$$

Note that because of the assumptions (140) and (139) we may replace $(\overline{v}_k)_{ij}^n$ by $\boldsymbol{V}_i^n \cdot \boldsymbol{n}_{ij}$ in (151), see Zein et al. [47], and, hence, conclude with (145)

$$(\alpha_k)_i^{n+1} = (\alpha_k)_i^n - \Delta t\, \boldsymbol{V}_i^n \cdot (\nabla \alpha_k)_i^n. \tag{152}$$

Plugging (145) into (133) we finally obtain the finite volume discretization. In particular, it can be written in divergence form

$$(\boldsymbol{u}_k)_i^{n+1} = (\boldsymbol{u}_k)_i^n - \frac{\Delta t}{|V_i|} \sum_{j \in \mathcal{N}(i)} |\Gamma_{ij}| (\boldsymbol{F}_k)_{ij}^n \tag{153}$$

with modified numerical flux

$$(\boldsymbol{F}_k)_{ij}^n = \boldsymbol{F}_k(\boldsymbol{w}_{ij}^n, \boldsymbol{w}_{ji}^n, \boldsymbol{n}_{ij}) - \boldsymbol{H}(\boldsymbol{w}_i^n)\, \boldsymbol{n}_{ij} \left((\overline{\alpha}_k)_{ij}^n - (\alpha_k)_i^n\right). \tag{154}$$

Note, however, that this discretization is not conservative because of the term $\boldsymbol{H}(\boldsymbol{w}_i^n)$, i.e., $(\boldsymbol{F}_k)_{ij}^n \neq -(\boldsymbol{F}_k)_{ji}^n$. The above discretization is appropriate in case of mechanical equilibrium because of (51). In the non-equilbrium case, we have to replace (154) by

$$(\boldsymbol{F}_k)_{ij}^n = \boldsymbol{F}_k(\boldsymbol{w}_{ij}^n, \boldsymbol{w}_{ji}^n, \boldsymbol{n}_{ij}) + \sum_{l=1, \neq k}^{K} \boldsymbol{H}_{k,l}(\boldsymbol{w}_i^n)\, \boldsymbol{n}_{ij} \left((\overline{\alpha}_l)_{ij}^n - (\alpha_l)_i^n\right). \tag{155}$$

B   HLLC Riemann Solver

The Riemann problem at the cell interfaces is not solved for the fully coupled system (2), (3), (4) and (6) but we only consider the fluid equations for mass, momentum and energy of the pure phases, where the volume fractions are considered to be frozen. Let be $\boldsymbol{n}$ normal to the interface. Thus we consider the following Cauchy problem in normal direction $\xi = \boldsymbol{x} \cdot \boldsymbol{n}$

$$\boldsymbol{u}_t + (\boldsymbol{F}(\boldsymbol{u}, \boldsymbol{\alpha}))_\xi = \boldsymbol{0}, \tag{156}$$

$$\boldsymbol{u}(0, \xi) = \begin{cases} \boldsymbol{u}_L & , \ \xi < 0 \\ \boldsymbol{u}_R & , \ \xi > 0 \end{cases}. \tag{157}$$

Here $\boldsymbol{u} = (\boldsymbol{u}_1^T, \dots, \boldsymbol{u}_K^T)^T$ denotes the vector of all conserved quantities of all phases composed of the vector $\boldsymbol{u}_k = \alpha_k (\rho_k, \rho_k \boldsymbol{v}_k^T, \rho_k E_k)^T$ of the conserved quantities of a pure phase k and $\boldsymbol{\alpha} = (\alpha_1, \dots, \alpha_K)^T$ is the vector of volume fractions. The flux $\boldsymbol{F} = (\boldsymbol{F}_{1,n}^T, \dots, \boldsymbol{F}_{K,n}^T)^T$ in normal direction $\boldsymbol{n}$ is defined by the corresponding fluxes for the pure phases

$$\boldsymbol{F}_{k,n} = \alpha_k \left(\rho_k v_{k,n}, \rho_k v_{k,n} \boldsymbol{v}_k^T + p_k \boldsymbol{n}^T, \rho_k v_{k,n} (E_k + p_k/\rho_k) \right)^T \tag{158}$$

with normal velocity $v_{k,n} = \boldsymbol{v}_k \cdot \boldsymbol{n}$. The solution of the Riemann problem (156) and (157) is approximated by the HLLC solver, i.e.,

$$\boldsymbol{u}(t, \xi) = \begin{cases} \boldsymbol{u}_L & , \ \xi/t < S_L \\ \boldsymbol{u}_{L*} & , \ S_L < \xi/t < S_* \\ \boldsymbol{u}_{R*} & , \ S_* < \xi/t < S_R \\ \boldsymbol{u}_R & , \ S_R < \xi/t \end{cases}, \tag{159}$$

where the intermediate states $\boldsymbol{u}_{L*}$, $\boldsymbol{u}_{R*}$ and the velocities S_L, S_* and S_R are to be appropriately determined. Here we proceed similar to the case of a single-phase fluid described in the Toro's book [45]. Starting point are the Rankine-Hugoniot jump conditions for the system (156)

$$\boldsymbol{F}_{K*} = \boldsymbol{F}_K + S_K (\boldsymbol{u}_{K*} - \boldsymbol{u}_K), \tag{160}$$

$$\boldsymbol{F}_{R*} = \boldsymbol{F}_{L*} + S_* (\boldsymbol{u}_{R*} - \boldsymbol{u}_{L*}), \tag{161}$$

where $K \in \{L, R\}$ represents the left and right state, respectively. These are three equations for four unknown vectors $\boldsymbol{u}_{K*}$ and $\boldsymbol{F}_{K*}$. The task is to find $\boldsymbol{u}_{K*}$ such that the fluxes $\boldsymbol{F}_{K*}$ satisfy the jump conditions (160) and (161), respectively. For this purpose, we assume that the following assumptions hold true for all phases $k = 1, \ldots, K$

$$p_{k,L*} = p_{k,R*} = p_{k,*}, \tag{162}$$

$$v_{kn,L*} = v_{kn,R*} = v_{kn,*}, \tag{163}$$

$$\alpha_{k,K*} = \alpha_{k,K}, \; K \in \{L, R\} \tag{164}$$

i.e., we assume pressure and velocity equilibrium and the volume fractions only jump across the contact discontinuity. Then by rearranging of (160) and assumptions (162), (163) and (164) we obtain

$$(S_K - v_{k,n,*}) \begin{pmatrix} \alpha_k \, \rho_k \\ \alpha_k \, \rho_k \, \boldsymbol{v}_k \\ \alpha_k \, \rho_k \, E_k \end{pmatrix}_{K*} =$$
$$(S_K - v_{k,n,K}) \begin{pmatrix} \alpha_k \, \rho_k \\ \alpha_k \, \rho_k \, \boldsymbol{v}_k \\ \alpha_k \, \rho_k \, E_k \end{pmatrix}_K + \begin{pmatrix} 0 \\ \alpha_{k,K} \, (p_{k,*} - p_{k,K}) \, \boldsymbol{n} \\ \alpha_{k,K} \, (v_{k,n,*} \, p_{k,*} - v_{k,n,K} \, p_{k,K}) \end{pmatrix} \tag{165}$$

¿From this relation we can deduce the intermediate states for density, momentum, and energy

$$\begin{pmatrix} \alpha_k \, \rho_k \\ \alpha_k \, \rho_k \, \boldsymbol{v}_k \\ \alpha_k \, \rho_k \, E_k \end{pmatrix}_{K*} = \tag{166}$$
$$(\alpha_k \, \rho_k)_K \, \frac{S_K - v_{k,n,K}}{S_K - v_{k,n,*}} \begin{pmatrix} 1 \\ \boldsymbol{v}_{k,K} + (v_{k,n,*} - v_{k,n,K}) \, \boldsymbol{n} \\ E_{k,K} + (v_{k,n,*} - v_{k,n,K}) \left(v_{k,n,*} + \frac{p_{k,K}}{\rho_{k,K} \, (S_K - v_{k,n,K})} \right) \end{pmatrix}$$

Here the intermediate density follows directly from (165). For the intermediate velocity state we first determine an intermediate pressure state where we multiply the momentum equation of (165) by $\boldsymbol{n}^T$ and use the assumptions (162), (163), (164) together with the intermediate density state:

$$(p_{k,*} - p_{k,K}) = \rho_{k,K} \, (v_{k,n,K} - S_K) \, (v_{k,n,K} - v_{k,n,*}). \tag{167}$$

The intermediate energy state then follows from (165) together with the intermediate pressure state (167) and assumptions (162), (163).

In order to derive S_* we assume that S_L and S_R are known. Then we conclude from the intermediate pressure state (167) and assumption (162)

$$S_{k,*} \equiv v_{k,n,*} = \frac{p_{k,L} - p_{k,R} - \rho_{k,L} \, v_{k,n,L} \, (S_L - v_{k,n,L}) + \rho_{k,R} \, v_{k,n,R} \, (S_R - v_{k,n,R})}{\rho_{k,R} \, (S_R - v_{k,n,R}) - \rho_{k,L} \, (S_L - v_{k,n,L})}. \tag{168}$$

Assuming pressure and velocity equilibrium with the mixture pressure and the mixture velocity, respectively, defined in (9), i.e.,

$$p_{K'}^{mix} = p_{1,K'} = \ldots = p_{K,K'}, \quad K' \in \{L, R\} \tag{169}$$

$$\boldsymbol{v}_{K'}^{mix} = \boldsymbol{v}_{1,K'} = \ldots = \boldsymbol{v}_{K,K'}, \quad K' \in \{L, R\} \tag{170}$$

we obtain for the still phase dependent intermediate wave speed

$$v_{k,n,*} = \frac{p_L^{mix} - p_R^{mix} - \rho_{k,L} \, v_{n,L}^{mix} \, (S_L - v_{n,L}^{mix}) + \rho_{k,R} \, v_{n,R}^{mix} \, (S_R - v_{n,R}^{mix})}{\rho_{k,R} \, (S_R - v_{n,R}^{mix}) - \rho_{k,L} \, (S_L - v_{n,L}^{mix})}. \tag{171}$$

Replacing the phase densities by the mixture density (9) we finally obtain one value for the intermediate wave speed S_*:

$$S_* = v_{n,*}^{mix} = \frac{p_L^{mix} - p_R^{mix} - \rho_L^{mix} \, v_{n,L}^{mix} \, (S_L - v_{n,L}^{mix}) + \rho_R^{mix} \, v_{n,R}^{mix} \, (S_R - v_{n,R}^{mix})}{\rho_R^{mix} \, (S_R - v_{n,R}^{mix}) - \rho_L^{mix} \, (S_L - v_{n,L}^{mix})} \tag{172}$$

It remains to fix the left and right wave speeds S_L and S_R. For this we follow the choice suggested by Davis [11], i.e.,

$$S_L = min_{k=1,\ldots,K}\{v_{k,n,L} - c_{k,L}, v_{k,n,R} - c_{k,R}\}, \tag{173}$$

$$S_R = max_{k=1,\ldots,K}\{v_{k,n,L} + c_{k,L}, v_{k,n,R} + c_{k,R}\}. \tag{174}$$

C Quasi-1D Scheme: Spherical Symmetry

Here we present the derivation of the quasi-1D scheme in analogy to previous work [6, 33]. The basic idea is to consider the full 3D scheme determined by the evolution equations for the conserved variables (153) of each phase k and the non-conservative volume fractions (152) for a special discretization that allows for spherical symmetry. For this purpose, we introduce the "mixed" vector of conserved and non-conserved quantities

$$\boldsymbol{w} = (\boldsymbol{\alpha}^T, \boldsymbol{u}_1^T, \ldots, \boldsymbol{u}_K^T)^T. \tag{175}$$

The corresponding evolution equations are determined by the coupled system determined by (52) and (53). Its finite volume discretization then reads

$$\boldsymbol{w}_i^{n+1} = \boldsymbol{w}_i^n - \frac{\Delta t}{|V_i|} \sum_{j \in \mathcal{N}(i)} |\Gamma_{ij}| \boldsymbol{G}(\boldsymbol{w}_i^n, \boldsymbol{w}_j^n, \boldsymbol{n}_{ij}) \tag{176}$$

where the numerical flux is defined as

$$\boldsymbol{G} = (\boldsymbol{G}_\alpha^T, \boldsymbol{G}_1^T, \ldots, \boldsymbol{G}_K^T)^T. \tag{177}$$

with

$$\boldsymbol{G}_\alpha(\boldsymbol{w}_i^n, \boldsymbol{w}_j^n, \boldsymbol{n}_{ij}) = (\boldsymbol{V}_I)_i^n \, \boldsymbol{n}_{ij} \, (\overline{\boldsymbol{\alpha}_k})_{ij}^n, \tag{178}$$

$$\boldsymbol{G}_k(\boldsymbol{w}_i^n, \boldsymbol{w}_j^n, \boldsymbol{n}_{ij}) = \boldsymbol{F}_k(\boldsymbol{w}_{ij}^n, \boldsymbol{w}_{ji}^n, \boldsymbol{n}_{ij}) + \sum_{l=1,\neq k}^K \boldsymbol{H}_{k,l}(\boldsymbol{w}_i^n) \, \boldsymbol{n}_{ij} \, (\overline{\alpha_l})_{ij}^n. \tag{179}$$

Here $\boldsymbol{w}_{ij}^n$ denotes some reconstructed value of cell V_i at the cell interface Γ_{ij}. For a first order reconstruction this coincides with the cell average, i.e., $\boldsymbol{w}_{ij}^n = \boldsymbol{w}_i^n$. Moreover the normal vectors at the interface only differ in sign, i.e., $\boldsymbol{n}_{ij} = -\boldsymbol{n}_{ji}$.

Let us note that the numerical flux is made of a conservative part $\boldsymbol{F}_k$ coming from the standard Godunov-type approach, i.e.,

$$\boldsymbol{F}_k(\boldsymbol{w}_i, \boldsymbol{w}_j, \boldsymbol{n}_{ij}) = -\boldsymbol{F}_k(\boldsymbol{w}_j, \boldsymbol{w}_i, \boldsymbol{n}_{ji}),$$

and a non-conservative part corresponding to the terms $\boldsymbol{H}_{k,l}(\boldsymbol{w}_i^n)$ and $(\boldsymbol{V}_I)_i^n$ coming from a simple upwind approximation of the transport equation.

Next, we apply this scheme to a special discretization where the underlying computational domain is the ball

$$B = \left\{(x, y, z), x^2 + y^2 + z^2 < R^2\right\}.$$

In order to mesh it, we consider spherical coordinates

$$x = r \cos \varphi \cos \theta, \quad y = r \sin \varphi \cos \theta, \quad z = r \sin \theta,$$

with parameters

$$0 \leq r \leq R, \quad -\frac{\pi}{2} \leq \theta \leq \frac{\pi}{2}, \quad -\pi \leq \varphi \leq \pi.$$

We now construct a regular discretization in spherical coordinates. For this purpose, we choose three integers N_r, N_θ, N_φ and introduce the step sizes

$$\Delta r := \frac{R}{N_r}, \quad \Delta \theta := \frac{\pi}{N_\theta}, \quad \Delta \varphi := \frac{2\pi}{N_\varphi}.$$

Note that in order to obtain the quasi-1D scheme, we will have to let tend $\Delta\theta$ and $\Delta\varphi$ to zero later on. The discretization of the parameter space is then determined by

$$
\begin{aligned}
r_i &:= (i+1/2)\Delta r, \quad i = 0, 1, \cdots \\
\theta_j &:= j\Delta\theta, \quad j = \cdots - 2, -1, 0, 1, 2, \cdots \\
\varphi_l &:= l\Delta\varphi, \quad l = \cdots - 2, -1, 0, 1, 2, \cdots
\end{aligned}
$$

By these grid points, we define the discretization in the parameter space by the cells

$$
C_{(i,j,l)} = (r_{i-1/2}, r_{i+1/2}) \times (\theta_{j-1/2}, \theta_{j+1/2}) \times (\varphi_{l-1/2}, \varphi_{l+1/2}).
$$

The discretization in the physical space is then determined by the cells

$$
V_{(i,j,l)} = \left\{ (r\cos\varphi\cos\theta, r\sin\varphi\cos\theta, r\sin\theta), \quad (r,\theta,\varphi) \in C_{(i,j,l)} \right\}.
$$

In order to obtain the quasi-1D scheme, we suppose that the approximate solution also satisfies a discrete rotational symmetry. More precisely, we suppose that

$$
\boldsymbol{v}_{k,(i,j,l)} = v_{kr,i}(\cos\varphi_l\cos\theta_j, \sin\varphi_l\cos\theta_j, \sin\theta_j)^T \tag{180}
$$

and also that

$$
\rho_{k,(i,j,l)} = \rho_{k,i} \quad p_{k,(i,j,l)} = p_{k,i} \quad \alpha_{k,(i,j,l)} = \alpha_{k,i} \tag{181}
$$

do not depend on (j, l). In this way, it is sufficient to write the scheme (176) on the cells $V_{(i,0,0)}$. This will permit to compute the one-dimensional solution through

$$
\boldsymbol{w}^n_{(i,0,0)} = ((\boldsymbol{\alpha}^n_i)^T, ((\boldsymbol{v}_1)^n_i)^T, \ldots, ((\boldsymbol{v}_K)^n_i)^T)^T, \tag{182}
$$

$$
\boldsymbol{v}^n_{k,i} = ((\alpha_k\rho_k)^n_i, (\alpha_k\rho_k v_{kr})^n_i, 0, 0, (\alpha_k\rho_k E_k)^n_i)^T. \tag{183}
$$

We denote by

Γ_W the (West) edge between the cells $V_{(i,0,0)}$ and $V_{(i-1,0,0)}$,

Γ_E the (East) edge between the cells $V_{(i,0,0)}$ and $V_{(i+1,0,0)}$,

Γ_N the (North) edge between the cells $V_{(i,0,0)}$ and $V_{(i,0,1)}$,

Γ_S the (South) edge between the cells $V_{(i,0,0)}$ and $V_{(i,0,-1)}$,

Γ_U the (Upper) edge between the cells $V_{(i,0,0)}$ and $V_{(i,1,0)}$,

Γ_B the (Bottom) edge between the cells $V_{(i,0,0)}$ and $V_{(i,-1,0)}$.

We take as a convention that the corresponding unit normal vectors are pointing toward the exterior of $V_{(i,0,0)}$. The finite volume scheme then reads

$$
\begin{aligned}
&\int_{V_{i,0,0}} \frac{\boldsymbol{w}^{n+1}_{(i,0,0)} - \boldsymbol{w}^n_{(i,0,0)}}{\Delta t} + \\
&\int_{\Gamma_W} \boldsymbol{G}(\boldsymbol{w}^n_{(i,0,0)}, \boldsymbol{w}^n_{(i-1,0,0)}, \boldsymbol{n}_W) + \int_{\Gamma_E} \boldsymbol{G}(\boldsymbol{w}^n_{(i,0,0)}, \boldsymbol{w}^n_{(i+1,0,0)}, \boldsymbol{n}_E) + \\
&\int_{\Gamma_N} \boldsymbol{G}(\boldsymbol{w}^n_{(i,0,0)}, \boldsymbol{w}^n_{(i,0,1)}, \boldsymbol{n}_N) + \int_{\Gamma_S} \boldsymbol{G}(\boldsymbol{w}^n_{(i,0,0)}, \boldsymbol{w}^n_{(i,0,-1)}, \boldsymbol{n}_S) + \\
&\int_{\Gamma_U} \boldsymbol{G}(\boldsymbol{w}^n_{i,0,0}, \boldsymbol{w}^n_{i,1,0}, \boldsymbol{n}_U) + \int_{\Gamma_B} \boldsymbol{G}(\boldsymbol{w}^n_{(i,0,0)}, \boldsymbol{w}^n_{(i,-1,0)}, \boldsymbol{n}_B) = \boldsymbol{0}.
\end{aligned}
$$

The important fact here is that for computing the North, South, Upper and Bottom fluxes we have to solve symmetric Riemann problems with two opposite normal velocities, cf. [6]. This is implied by the discrete rotational symmetry condition (180). In particular, the velocities in longitudinal and circumferential direction inside the cell $V_{i,0,0}$ vanish, i.e.,

$$
\boldsymbol{v}_{k,(i,0,0)} = (v_{kr}, 0, 0)^T. \tag{184}
$$

The corresponding numerical fluxes corresponding to a single phase are then of the form

$$\boldsymbol{F}_k(\boldsymbol{w}_L, \boldsymbol{w}_R, \boldsymbol{n}) = (\alpha_k \rho_k v_{kn}^*, v_{kn}^* \boldsymbol{v}_k^* \alpha_k p_k^* \boldsymbol{n}^T, 0)^T = (0, \alpha_k p_k^* \boldsymbol{n}^T, 0)^T$$

where p_k^* and $\boldsymbol{v}_k^* = \boldsymbol{0}$, $v_{kn}^* = \boldsymbol{v}_k^* \cdot \boldsymbol{n} = 0$ are the pressure and the velocity between the two symmetric rarefaction waves in the Riemann problem solution. Note that due to the rotational symmetry condition (181) there are common values for $\rho_k = \rho_{k,L} = \rho_{k,R}$, $p_k = p_{k,L} = p_{k,R}$ and $\boldsymbol{\alpha}_k = \boldsymbol{\alpha}_{k,L} = \boldsymbol{\alpha}_{k,R}$. Together with (184) the mixture source terms then read

$$\boldsymbol{H}_{k,l} \boldsymbol{n} = (0, P_{k,l} \boldsymbol{n}^T, P_{k,l} V_{I,n})^T = (0, P_{k,l} \boldsymbol{n}^T, 0)^T.$$

For the composed numerical fluxes (179) and (178) we thus conclude

$$\boldsymbol{G}_\alpha(\boldsymbol{w}_L, \boldsymbol{w}_R, \boldsymbol{n}) = V_n \boldsymbol{\alpha}_k = \boldsymbol{0}, \tag{185}$$

$$\boldsymbol{G}_k(\boldsymbol{w}_L, \boldsymbol{w}_R, \boldsymbol{n}) = (0, \alpha_k p_k^* \boldsymbol{n}^T, 0)^T + \sum_{l=1, \neq k}^{K} (0, P_{k,l} \boldsymbol{n}^T, 0)^T \alpha_l. \tag{186}$$

In addition, the pressure p_k^* tends to the common pressure $p_k = p_{k,L} = p_{k,R}$ when $\Delta\theta \to 0$ and $\Delta\varphi \to 0$. Note, that the discrete geometric source term will come from these North, South, Upper and Bottom edges.

Introducing the volume $\Delta r^3 := \frac{1}{3}(r_{i+1/2}^3 - r_{i-1/2}^3)$ and the interface area by $r_{i+1/2}^2$, then by Taylor expansions for small $\Delta\varphi$ and $\Delta\theta$ the scheme can also be written as

$$\Delta r^3 \Delta\varphi \Delta\theta \frac{\boldsymbol{w}_{i,0,0}^{n+1} - \boldsymbol{w}_{i,0,0}^n}{\Delta t} +$$

$$r_{i+1/2}^2 \Delta\varphi \Delta\theta \boldsymbol{G}(\boldsymbol{w}_{i,0,0}^n, \boldsymbol{w}_{i-1,0,0}^n, (-1,0,0)^T) +$$

$$r_{i-1/2}^2 \Delta\varphi \Delta\theta \boldsymbol{G}(\boldsymbol{w}_{i,0,0}^n, \boldsymbol{w}_{i+1,0,0}^n, (1,0,0)^T) +$$

$$\Delta r^3 \Delta\theta (\boldsymbol{0}^T, (0, -(\alpha_k p_k)_i^n \frac{\Delta\varphi}{2}, (\alpha_k p_k + \sum_{l=1,\neq k}^K P_{k,l}\alpha_l)_i^n, 0, 0)_{k=1,\dots,K})^T +$$

$$\Delta r^3 \Delta\theta (\boldsymbol{0}^T, (0, -(\alpha_k p_k)_i^n \frac{\Delta\varphi}{2}, -(\alpha_k p_k + \sum_{l=1,\neq k}^K P_{k,l}\alpha_l)_i^n, 0, 0)_{k=1,\dots,K})^T +$$

$$\Delta r^3 \Delta\varphi (\boldsymbol{0}^T, (0, -(\alpha_k p_k)_i^n \frac{\Delta\theta}{2}, 0, (\alpha_k p_k + \sum_{l=1,\neq k}^K P_{k,l}\alpha_l)_i^n, 0)_{k=1,\dots,K})^T) +$$

$$\Delta r^3 \Delta\varphi (\boldsymbol{0}^T, (0, -(\alpha_k p_k)_i^n \frac{\Delta\theta}{2}, 0, -(\alpha_k p_k + \sum_{l=1,\neq k}^K P_{k,l}\alpha_l)_i, 0)_{k=1,\dots,K})^T =$$

$$o(\Delta\varphi^2 + \Delta\theta^2).$$

Dividing by $\Delta\varphi \Delta\theta$ and passing to the limit, we finally obtain

$$\boldsymbol{w}_{(i,0,0)}^{n+1} = \boldsymbol{w}_{(i,0,0)}^n -$$

$$\frac{\Delta t}{\Delta r^3} \left(\boldsymbol{G}(\boldsymbol{w}_{(i,0,0)}^n, \boldsymbol{w}_{(i+1,0,0)}^n, (1,0,0)^T) + \boldsymbol{G}(\boldsymbol{w}_{(i,0,0)}^n, \boldsymbol{w}_{(i-1,0,0)}^n, (-1,0,0)^T) \right) +$$

$$\frac{\Delta r \Delta t}{\Delta r^3} (\boldsymbol{0}^T, (0, 2\hat{r}_i (\alpha_k p_k)_i^n, 0, 0, 0)_{k=1,\dots,K})^T$$

with the cell center $\hat{r}_i := \frac{1}{2}(r_{i+1/2} + r_{i-1/2})$.

Removing the momentum equations in longitudinal and circumferential direction in the mixed vector $\boldsymbol{w}$ in (175) we finally conclude with the quasi-1D scheme

$$\boldsymbol{w}_i^{n+1} = \boldsymbol{w}_i^n - \frac{\Delta t}{\Delta r^3} \left(r_{i+\frac{1}{2}} \boldsymbol{G}(\boldsymbol{w}_i^n, \boldsymbol{w}_{i+1}^n) - r_{i-\frac{1}{2}} \boldsymbol{G}(\boldsymbol{w}_{i-1}^n, \boldsymbol{w}_i^n) \right) + \frac{\Delta r \, \Delta t}{\Delta r^3} \boldsymbol{S}_i^n, \tag{187}$$

where the numerical flux is defined according to (177) with

$$\boldsymbol{G}_\alpha(\boldsymbol{w}_i^n, \boldsymbol{w}_j^n) \;=\; V_{ri}^n \, (\overline{\boldsymbol{\alpha}_k})_{ij}^n, \tag{188}$$

$$\boldsymbol{G}_k(\boldsymbol{w}_i^n, \boldsymbol{w}_j^n) \;=\; \boldsymbol{F}_k(\boldsymbol{w}_{ij}^n, \boldsymbol{w}_{ji}^n) + \sum_{l=1,\neq k}^{K} \boldsymbol{H}_{k,l}(\boldsymbol{w}_i^n) \, (\overline{\alpha_l})_{ij}^n \tag{189}$$

and

$$\boldsymbol{F}_k(\boldsymbol{w}_L, \boldsymbol{w}_R) = \boldsymbol{f}_k(\overline{w}) \;=\; \overline{\alpha_k \rho_k v_{kr}}(1, \overline{v_{kr}}, \overline{E_k} + \overline{p_k}/\overline{\rho_k})^T + (0, \overline{\alpha_k p_k}, 0)^T \tag{190}$$

$$\boldsymbol{H}_{k,l}(\boldsymbol{w}) \;=\; (0, P_{k,l}, P_{k,l} V_{I,r})^T. \tag{191}$$

In case of pressure equilibrium, the numerical fluxes $\boldsymbol{G}_k$ simplify to

$$\boldsymbol{G}_k(\boldsymbol{w}_i^n, \boldsymbol{w}_j^n) = \boldsymbol{F}_k(\boldsymbol{w}_{ij}^n, \boldsymbol{w}_{ji}^n) - \boldsymbol{H}(\boldsymbol{w}_i^n) \, (\overline{\alpha_k})_{ij}^n$$

with

$$\boldsymbol{H}(\boldsymbol{w}) = (0, p, p V_{I,r})^T,$$

because of (51) and (188). The numerical source term due to the change in the metric reads

$$\boldsymbol{S} = (\boldsymbol{S}_\alpha^T, \boldsymbol{S}_1^T, \ldots, \boldsymbol{S}_K^T)^T. \tag{192}$$

with

$$\boldsymbol{S}_\alpha(\boldsymbol{w}_i^n) \;=\; \boldsymbol{0}, \tag{193}$$

$$\boldsymbol{S}_k(\boldsymbol{w}_i^n) \;=\; (0, 2\hat{r}_i(\alpha_k p_k)_i^n, 0)^T. \tag{194}$$

In particular, we note that there is no metric source term in the quasi-one-dimensional discretization of the volume fractions.